

AD-A158 037

SENSITIVITY TO MEAN FLOW PARAMETERS OF THE LOW
WAVENUMBER CONTENT OF THE (U) CAMBRIDGE ACOUSTICAL
ASSOCIATES INC MA J E COLE 26 APR 85 CAA-U-1205-333

1/1

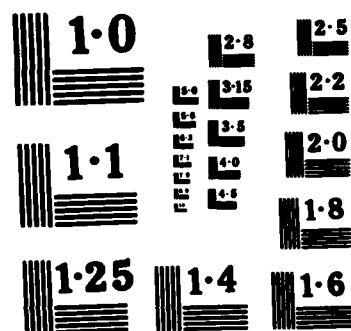
UNCLASSIFIED

DTNSRDC-2280 N00014-84-C-0141

F/G 20/4

NL

					END								
					FILED								
					DTIC								



NATIONAL BUREAU OF STANDARDS
MICROCOPY RESOLUTION TEST CHART

AD-A158 037

CAMBRIDGE ACOUSTIC ASSOCIATES

SENSITIVITY TO MEAN FLOW PARAMETERS OF THE
LOW WAVENUMBER CONTENT OF THE WALL PRESSURE UNDER
A TURBULENT BOUNDARY LAYER

Prepared by
J. E. Cole, III

April 1985

DTIC
ELECTE
AUG 19 1985
A

Final Report U-1205-333

DTIC FILE COPY

This research was sponsored by the Naval Sea Systems Command General Hydromechanics Research (GHR) Program administered by the David W. Taylor Naval Ship Research and Development Center (DTNSRDC) under Contract N00014-84-C-0141

Cambridge Acoustical Associates, Inc.
54 CambridgePark Drive
Cambridge, Massachusetts 02140

This document has been approved
for public release and sale; its
distribution is unlimited.

54 CAMBRIDGE PARK DRIVE, CAMBRIDGE, MASSACHUSETTS 02140

85 816 032

UNCLASSIFIED

SECURITY CLASSIFICATION OF THIS PAGE

AD-A158037

REPORT DOCUMENTATION PAGE				
1a REPORT SECURITY CLASSIFICATION UNCLASSIFIED		1b RESTRICTIVE MARKINGS N/A		
2a SECURITY CLASSIFICATION AUTHORITY N/A		3 DISTRIBUTION/AVAILABILITY OF REPORT APPROVED FOR PUBLIC RELEASE; DISTRIBUTION UNLIMITED		
2b DECLASSIFICATION/DOWNGRADING SCHEDULE N/A				
4 PERFORMING ORGANIZATION REPORT NUMBER(S) U-1205-333		5 MONITORING ORGANIZATION REPORT NUMBER(S) #2280		
6a NAME OF PERFORMING ORGANIZATION CAMBRIDGE ACOUSTICAL ASSOC, INC.		6b OFFICE SYMBOL (if applicable)		7a NAME OF MONITORING ORGANIZATION DAVID W. TAYLOR NAVAL SHIP R&D CENTER Code 1504 (1505)
6c ADDRESS (City, State, and ZIP Code) 54 CAMBRIDGE PARK DRIVE CAMBRIDGE, MA 02140		7b ADDRESS (City, State, and ZIP Code) BETHESDA, MARYLAND 20084-5000		
8a NAME OF FUNDING/SPONSORING ORGANIZATION NAVAL SEA SYSTEMS COMMAND		8b OFFICE SYMBOL (if applicable) SEA05R24		9. PROCUREMENT INSTRUMENT IDENTIFICATION NUMBER Contract Number - N00014-84-C-0141
8c ADDRESS (City, State, and ZIP Code) Washington, D.C. 20360		10 SOURCE OF FUNDING NUMBERS		
		PROGRAM ELEMENT NO. 61153N	PROJECT NO. SR 023 01	TASK NO. 23454 WORK UNIT ACCESSION NO. N/A
11 TITLE (Include Security Classification) SENSITIVITY TO MEAN FLOW PARAMETERS OF THE LOW WAVENUMBER CONTENT OF THE WALL PRESSURE UNDER A TURBULENT BOUNDARY LAYER				
12 PERSONAL AUTHOR(S) John E. Cole, III				
13a TYPE OF REPORT FINAL		13b TIME COVERED FROM 83,12,1 TO 85,5,31		14 DATE OF REPORT (Year, Month, Day) 1985, 4, 26
15 PAGE COUNT 44				
16 SUPPLEMENTARY NOTATION Sponsored under the Naval Sea Systems Command General Hydromechanics Research (GHR) Program administered by the David Taylor Naval Ship R&D Center, Code 1504 (1505), Bethesda, MD 20084-5000				
17 COSATI CODES			18 SUBJECT TERMS (Continue on reverse if necessary and identify by block number)	
FIELD	GROUP	SUB-GROUP		
20	04	Hydro	GHR Program, Turbulent Boundary Layer, Low Wavenumber, Wall- Pressure Fluctuations.	
19 ABSTRACT (Continue on reverse if necessary and identify by block number) The objective of this study is to examine the sensitivity of the low wavenumber portion of the wall pressure field under a turbulent boundary layer to both flow and wall conditions. The analytical procedure makes use of a method for calculating the broadband correlation function of the wall pressure field in which the specific flow characteristics enter through profiles of the mean velocity shear and turbulence intensity across the boundary layer. The basic assumption used to extend the results of this procedure to narrowband frequency characteristics is that there is a range of large spatial separations in which Strouhal scaling is not important. Several specific boundary layers are considered including flows on smooth and rough walls and in zero, favorable, and adverse pressure gradients. Results are presented for the point pressure, the spatial correlation function, and the low wavenumber spectral level. <i>Hydrodynamic</i>				
20 DISTRIBUTION/AVAILABILITY OF ABSTRACT <input checked="" type="checkbox"/> UNCLASSIFIED/UNLIMITED <input type="checkbox"/> SAME AS RPT <input type="checkbox"/> DTIC USERS			21 ABSTRACT SECURITY CLASSIFICATION UNCLASSIFIED	
22a NAME OF RESPONSIBLE INDIVIDUAL Mr. V. J. Monacella			22b TELEPHONE (Include Area Code) 202-227-1503	
			22c OFFICE SYMBOL Code 1504/1505	

DD FORM 1473, 84 MAR

83 APR edition may be used until exhausted

All other editions are obsolete

SECURITY CLASSIFICATION OF THIS PAGE
UNCLASSIFIED

SENSITIVITY TO MEAN FLOW PARAMETERS OF THE
LOW WAVENUMBER CONTENT OF THE WALL PRESSURE UNDER
A TURBULENT BOUNDARY LAYER

Prepared by
J. E. Cole, III

April 1985

Final Report U-1205-333

This research was sponsored by the Naval Sea Systems Command
General Hydromechanics Research (GHR) Program administered
by the David W. Taylor Naval Ship Research and Development
Center (DTNSRDC) under Contract N00014-84-C-0141

Cambridge Acoustical Associates, Inc.
54 CambridgePark Drive
Cambridge, Massachusetts 02140



TABLE OF CONTENTS

	<u>Page</u>
ABSTRACT	iii
I. INTRODUCTION	1
II. ANALYTICAL MODEL	
A. Definitions	3
B. Scaling	4
C. Low Wavenumber Assumptions and Spectrum	4
D. Spatial Correlation Function	7
III. NUMERICAL EVALUATION	
A. Universal Functions	10
B. Turbulent Boundary Layer Data	
1. Data Sources	10
2. Data Curve Fit	
a. Turbulence Intensity	11
b. Mean Velocity Shear	12
3. Data Interface with Numerical Integration	
Integration	14
C. Wavenumber Spectrum	14
IV. RESULTS	15
V. CONCLUSIONS	19
TABLE I - BOUNDARY LAYER PARAMETERS	20
TABLE II - CALCULATED RATIO OF RMS SURFACE PRESSURE TO WALL SHEAR STRESS	21
FIGURES	22-38
REFERENCES	39

ABSTRACT

The objective of this study is to examine the sensitivity of the low wavenumber portion of the wall pressure field under a turbulent boundary layer to both flow and wall conditions. The analytical procedure makes use of a method for calculating the broadband correlation function of the wall pressure field in which the specific flow characteristics enter through profiles of the mean velocity shear and turbulence intensity across the boundary layer. The basic assumption used to extend the results of this procedure to narrowband frequency characteristics is that there is a range of large spatial separations in which Strouhal scaling is not important. Several specific boundary layers are considered including flows on smooth and rough walls and in zero, favorable, and adverse pressure gradients. Results are presented for the point pressure, the spatial correlation function, and the low wavenumber spectral level.

I. INTRODUCTION

When a turbulent boundary layer develops along a surface, the surface is acted upon by the pressure fluctuations generated by the flow. The resulting response of the surface and the pressure field it generates in many circumstances is an important noise source. The characteristics of the pressure fluctuations beneath a turbulent boundary layer (TBL) have therefore been a subject of interest for many years.

Perhaps the simplest conceptual model of the turbulent flow in boundary layer is that of frozen turbulence in which a pattern of random pressure field is convected by the flow past the boundary surface. Any pressure fluctuation of temporal frequency f that is present in this field would then have a spatial wavelength of $\lambda_c = U_c/f$, where U_c is the convection speed of the pattern. The associated convective wavenumber is

$$k_c = \frac{2\pi}{\lambda_c} = \frac{\omega}{U_c}$$

In underwater applications where flow speeds are relatively low and frequencies of interest can be relatively high, the convective wavelength is small (and, conversely the wavenumber is large). For example when $U_c = 20$ kt, $\lambda_c \approx 0.40$ in. at 1000 Hz. Because of their small wavelength, the noise associated with pressure disturbances having spatial scales comparable to λ_c is relatively easy to control by separating the flow from surfaces of interest by thin intermediate layers.

Although measurements of the spatial scales of the pressure field beneath turbulent boundary layers confirm that the spatial scale of most of the fluctuations is near the convective wavelength, there is present to some degree a broad distribution of wavelengths. In particular, a small portion of the pressure field exists in disturbances with long wavelengths (i.e., low wavenumbers). When the scale of the pressure field exceeds the convective wavelength by the Mach number (i.e., $M = U_c/c_o$, where c_o is the sound speed in the fluid), the boundary layer noise cannot be distinguished from an acoustic pressure disturbance of the same frequency. The level of the pressure fluctuations of the TBL having low wavenumber spatial scales therefore sets a noise floor for acoustic measurements made in proximity to the flow.

Because the low wavenumber content of the wall pressure field is small compared with the portion near the convective wavenumber, it has been difficult to establish the level of the low wavenumber spectrum. Measurements making use of wave-vector filters to reject the high wavenumber components have been successful in setting levels in small ranges of wavenumber at moderately low wavenumbers (e.g., 3 in^{-1} (Ref. 1)). These measurements however have been insufficient for determining the shape of the low wavenumber spectrum. The conclusion drawn from theoretical arguments based on a planar incompressible boundary layer of infinite extent is that the wavenumber spectrum should behave as k^2 in the low wavenumber range. An analytical model of the entire wavenumber spectrum of the wall pressure fluctuations that embodies this dependence is defined in Ref. 2.

The objective of the present study is to examine the sensitivity of the low wavenumber portion of the wall pressure field under a TBL to flow and wall conditions. The procedure makes use of an existing analytical method for calculating the broadband spatial correlation function.³ This method, which assumes a planar flow, is attractive because it is formulated explicitly in terms of the profiles of mean velocity and turbulence intensity across the boundary layer. The wavenumber spectrum is obtained from the Fourier transformation of the correlation function. Although the procedure is exact for broadband properties, it is argued that in the range of low wavenumber and frequency where Strouhal scaling is not expected, the broadband and narrowband spatial characteristics should be nearly the same. With this approximation the procedure is used to examine flow with both zero (i.e., nearly planar) and non-zero (i.e., substantially non-planar) pressure gradients.

A preliminary study using the proposed method is reported in Ref. 4 in which the shear contribution of the wall pressure field is examined for the flow over a smooth wall in zero pressure gradient. In the present study results for both shear and turbulence contributions are calculated for four different boundary layer flows. Two of these are non-planar, and although this violates an assumption of the analysis, they are included to evaluate the effect of a reasonably large variation in mean boundary layer properties on the results.

II. ANALYTICAL MODEL

A. Definitions

Both temporal and spatial characteristics of the wall pressure field under a TBL are determined from the second-order statistics of the field. Specifically the space-time correlation function of the pressure field is defined as follows:

$$C_{pp}(\bar{x}, \bar{\xi}, t, \tau) = E[p(\bar{x}, t)p(\bar{x} + \bar{\xi}, t + \tau)] \quad (1)$$

where $\bar{\xi}$ is the spatial separation vector, τ is the time delay, and E is the expected value. Under the assumptions of spatial and temporal stationarity, the correlation function becomes only a function of separation and is symmetric about zero. Furthermore as commonly implemented the expected value is taken to be the time average. When separation time τ is zero, we obtain the broadband correlation function

$$C_{pp}(\bar{\xi}, 0) = \langle p^2 \rangle R(\bar{\xi}) \quad (2)$$

where the first quantity is the mean-square pressure and $R(\bar{\xi})$ is the spatial correlation function normalized to unity at zero spatial separation.

Narrowband frequency information is obtained by Fourier transforming the temporal correlation function. For example the cross-spectral density is defined as the temporal transform of the space-time correlation function,

$$C_{pp}(\bar{\xi}, \omega) = \int_{-\infty}^{\infty} C_{pp}(\bar{\xi}, \tau) e^{-i\omega\tau} d\tau \quad (3)$$

A normalized cross-spectral density can be defined analogous to Eq. 2 such that

$$C_{pp}(\bar{\xi}, \omega) = P(\omega) R(\bar{\xi}, \omega) \quad (4)$$

where $R(0, \omega) = 1$.

The spatial Fourier transform of either Eqs. 2 or 4 yields the wavenumber spectrum of the pressure field. For example when Eq. 4 is transformed, the wavenumber-frequency spectrum is obtained,

$$\Phi(\bar{k}, \omega) = \int_{-\infty}^{\infty} C_{pp}(\bar{\xi}, \omega) e^{i\bar{k} \cdot \bar{\xi}} d\bar{\xi} \quad (5)$$

where the integral is over all separations on the surface. Owing to the symmetry of the cross-spectral density, the Fourier transform can be replaced by a cosine transform. This particular function is useful for describing the characteristics of the wall pressure field.

B. Scaling

Dimensionless parameters that characterize the wall pressure field of the TBL are obtained by selecting appropriate length and time scales. For this study we choose for these scales the outer parameters of displacement thickness δ_1 and mean flow speed U_o . From these parameters two length scales can be defined, one being δ_1 and the second being U_o/ω . The reciprocal of the latter is a wavenumber proportional to the convective wavenumber ($k_c = \omega/U_c$, where $U_c \approx .6 U_o$). For underwater applications these two length scales are quite disparate. The cross-spectral density from Eq. 4 can then be non-dimensionalized as follows:

$$\tilde{C}_{pp} = \frac{C_{pp}(\bar{\xi}, \omega) U_o}{q^2 \delta_1} = \tilde{P}(\omega \delta_1 / U_o) R(\omega \bar{\xi} / U_o, \bar{\xi} / \delta_1) \quad (6)$$

where $q = 1/2 \rho_o U_o^2$.

C. Low Wavenumber Assumptions and Spectrum

The boundary layer is assumed to be an incompressible flow acting on an infinite plane. Additionally changes along the flow direction are neglected in comparison with changes across the boundary layer. This latter assumption is compatible with the previous assumption of spatial stationarity. Under these conditions, the theorem of Kraichnan and Phillips⁵ that there is no net force on the plane generated by the TBL is applicable. A statement of this theorem applied to narrow frequency bands is

$$\int_{-\infty}^{\infty} C_{pp}(\bar{\xi}, \omega) d\bar{\xi} = 0 \quad (7)$$

An equivalent statement using Eq. 4 is that the wavenumber-frequency spectrum must vanish at zero wavenumber.

The low spatial wavenumber levels of the pressure field under a TBL reflect the information from the correlation measurements made at large separation distances. At large separations however, it is unlikely that the Strouhal dependence appearing in Eq. 6 remains as an important parameter. The standard conceptual argument against preserving Strouhal scaling in this limit is that it would imply low-frequency correlation of the wall pressure field at very large separations. Given the distortion to boundary layers due to shear, however this sustained correlation is not likely to exist.⁶

The experimental results for the scaling of the large separation narrow-band correlation are somewhat conflicting. Lack of Strouhal scaling in a low frequency/large separation regime has been reported in several experimental studies.⁶⁻⁸ Additionally, the analytical model developed by Chase² is consistent with the data trends of Bull.⁷ Measurements reported in Refs. 9 and 10 however do not indicate a lack of Strouhal scaling at low frequency. One explanation by Blake¹⁰ of this discrepancy with the results of Bull is that the latter data are distorted by the bandwidth of a filter in the measurements system.

In the present study we assume that there is a frequency/separation regime in which Strouhal scaling fails and we examine the implications to the (narrowband) wavenumber-frequency spectrum. Under this assumption, the cross-spectral density in Eq. 6 is given by

$$\begin{aligned} \tilde{C}_{pp}(\xi, \eta; \omega) &= \tilde{P}(\omega \delta_1 / U_o) R(\xi / \delta_1, \eta / \delta_1) \quad ; \\ \xi &> \xi_L \\ \eta &> \eta_L \end{aligned} \quad (8)$$

where ξ and η are the separation distances in the flow and transverse directions, respectively, and the subscript L indicates the separation beyond which Strouhal scaling fails. It is understood that the frequency range in Eq. 8 is also limited by the assumed lack of Strouhal scaling.

When both sides of Eq. 8 are integrated over frequency the simplification introduced by the assumed independence of Strouhal scaling becomes apparent. The result is the definition of the broadband spatial correlation function given in Eq. 2. Consequently, under the assumption of no Strouhal scaling the spatial characteristics of the wall pressure field at large separation become independent of the frequency bandwidth.

The wavenumber frequency spectrum is obtained from the two-dimensional Fourier transform of the cross-spectral density function. The integrals are over all separation distances and involve contributions from both large and small separation distances. In particular the narrowband wavenumber spectrum contains contributions from the narrowband correlation function at small separations which involves Strouhal scaling (i.e., Eq. 6). Invoking Eq. 8, we obtain the following expression for the narrowband wavenumber spectrum:

$$\begin{aligned} \tilde{\Phi}(k_1, k_2; \omega) = 4\tilde{P}(\omega) & \left[\int_0^{\xi_L} \int_0^{\eta_L} R(\xi, \eta, \omega/U_0) \cos k_1 \xi \cos k_2 \eta d\xi d\eta \right. \\ & \left. + \int_{\xi_L}^{\infty} \int_{\eta_L}^{\infty} R(\xi, \eta) \cos k_1 \xi \cos k_2 \eta d\xi d\eta \right] \end{aligned} \quad (9)$$

The Kraichnan-Phillips theorem expressed in Eq. 7 states that this spectrum must be zero at $k_1 = 0$. When applied to Eq. 9 as well as to its broadband counterpart, this theorem gives the following identity:

$$\int_0^{\xi_L} \int_0^{\eta_L} R(\xi, \eta, \omega/U_0) \cos k_2 \eta d\xi d\eta = \int_0^{\xi_L} \int_0^{\eta_L} R(\xi, \eta) \cos k_2 \eta d\xi d\eta \quad (10)$$

This equality states that the average over ξ of the narrowband and broadband correlation functions at small separations are equal. By Eq. 9 each of these contributions equals the negative of the ξ -average over large separations.

The relationship in Eq. 10 strictly applies to zero wavenumber (k_1). We assume that a similar relationship between integrals of the narrowband and broadband correlation function exists at small but non-zero wavenumber. Under this assumption the low wavenumber integral can be replaced by its broadband counterpart, giving the following approximate result for the low wavenumber-frequency spectrum:

$$\lim_{\substack{k_1 \rightarrow 0 \\ k_2 \rightarrow 0}} \tilde{\Phi}(k_1, k_2; \omega) = 4\tilde{P}(\omega) \int_0^{\infty} \int_0^{\infty} R(\xi, \eta) \cos k_1 \xi \cos k_2 \eta d\xi d\eta \quad (11)$$

This result is used in this report to obtain the low wavenumber frequency spectrum from a model of the broadband correlation function $R(\xi, \eta)$.

D. Spatial Correlation Function

The broadband spatial correlation function in Eq. 11 is evaluated using the analytical procedure developed in Ref. 3 by Meecham and Tavis which assumes the turbulent boundary layer to be a planar incompressible flow. The formalism and numerical results to facilitate implementation of the procedure are also given in Ref. 3; consequently, only an outline of the method is given here.

The pressure field in the incompressible boundary layer is governed by the following equation:

$$\nabla^2 p = -\rho_o \frac{\partial^2 H_{\alpha\beta}(\underline{r}')}{\partial r'_\alpha \partial r'_\beta} \quad (12)$$

where the subscripted variables are Cartesian tensors with indices 1 and 3 referring to the flow and normal directions, respectively, and the underlined variables are vectors. The source term on the right-hand side is given by

$$H_{\alpha\beta}(\underline{r}') = 2U(z')\delta_{\alpha 1}U_\beta + u_\alpha u_\beta - \langle u_\alpha u_\beta \rangle \quad (13)$$

where $\delta_{ij} = 1$ is the Kronecker delta function ($\delta_{ij} = 1, i=j; \delta_{ij} = 0, i \neq j$), U and u are the mean and fluctuating flow speeds, respectively, and z is the coordinate in the normal direction. This equation which holds in the semi-infinite space above a rigid wall is solved in terms of an infinite space Green's function by replacing the wall by an image source field and a drag force. The latter quantity is shown in Ref. 3 to be negligible. Under these conditions the solution for the pressure field in the boundary layer is given by

$$p(\underline{r}) = \frac{\rho_o}{4\pi} \int |\underline{r} - \underline{r}_o|^{-1} \frac{\partial^2 H_{\alpha\beta}(\underline{r}_o) d\underline{r}_o}{\partial r_{o\alpha} \partial r_{o\beta}} \quad (14)$$

where integral is over all space.

The normalized correlation function defined by Eqs. 1 and 2 is obtained by time-averaging the product of the pressures at two spatial locations,

$$C_{pp}(\underline{r}, \underline{r}') = \langle p(\underline{r}) p(\underline{r}') \rangle \quad (15)$$

When Eq. 14 is substituted into Eq. 15, the correlation is expressed in terms of a 2-fold volume (i.e., 6-fold linear) integral with multiple point velocity correlations appearing in the integrand. Simplifications are introduced by using the assumption of isotropic turbulence to model these correlation functions. The scale of the turbulence is taken to depend on the distance from the wall. Furthermore under the assumption of a Gaussian distribution function, fourth-order velocity correlations are expressed in terms of second-order correlations. With this assumption and extensive manipulations four of the integrals can be evaluated analytically in terms of relatively simple functions of the velocity correlations. The remaining two-fold integrals have to be evaluated numerically.

Two contributions to the correlation of the surface pressure are obtained. The first which depends on the correlation of the fluctuating velocity components is given by

$$R_{pp}^{(2)}(\eta) \equiv \frac{C_{pp}^{(2)}(\eta)}{q^2} = \frac{1}{\pi^2} \int_{-\infty}^{\infty} d\xi_3 [u'(|\xi_3|)/U_o]^4 / M \int_{-\eta}^{\infty} Q(\eta, \Delta, \zeta_3) d\Delta \quad (16)$$

where Q is an explicit function given in Ref. 3 in terms of several tabulated functions, M is the scaling function, and ξ_3, Δ are transformed separation coordinates. This contribution has been shown to be small in general. Results for the contribution of this term to the mean square pressure are presented in Section IV. The second contribution to the correlation depends on the product of the mean velocity gradient and the turbulence velocity. This contribution can be expressed as follows:

$$R_{pp}^{(1)}(\xi, \eta) \equiv \frac{C_{pp}^{(1)}(\xi, \eta)}{q^2} = \frac{8}{\pi} \int_0^{\infty} d\zeta_3 \left[\frac{d}{d\zeta_3} \left(\frac{U(\zeta_3)}{U_o} \right) \frac{u(\zeta_3)}{U_o} \right]^2 \int_0^{\infty} N(\xi, \eta, \rho, \zeta_3) \rho d\rho \quad (17)$$

where N is defined in terms of several tabulated functions, and ρ, ζ_3 are transformed separation coordinates.

As indicated in Eqs. 16 and 17, the spatial correlation of the wall pressure is given in terms of two-fold integrals that have to be evaluated numerically. The inner integral is a "universal" function in that it is

independent of specific boundary layer parameters. In this formulation variations between boundary layers introduced by roughness or pressure gradients are obtained through the profiles of mean velocity and of turbulence intensity that appear in the outer integral.

III. NUMERICAL EVALUATION

A. Universal Functions

The functions Q and N in the inner integrand of Eqs. 16 and 17 are defined in Ref. 3 in terms of explicit integrals of functions of the velocity correlations. A smooth representation of the velocity correlation function which is required to evaluate these integrals is used in Ref. 3. This reference also contains all the functions required to calculate Q and N both in graphical and in tabular form. In the present study the tabulated data are used to calculate the required integrals, these data being interpolated using third-order Lagrange and logarithmic (for large arguments of monotonically decreasing functions) interpolation schemes. The inner integral in Eqs. 16 and 17 is evaluated using Simpson's rule.

B. Turbulent Boundary Layer Data

1. Data Sources

The mean flow data required in the analytical calculation are the profiles of turbulence intensity and mean velocity shear across the boundary layer. For the purpose of the present study these data are required for flows over smooth and rough flat walls with pressure gradients that range from favorable to adverse. Sets of measurements that include both turbulence and mean velocity data for these conditions are limited to a small number of studies. Data for zero pressure gradient flows on a smooth wall from a number of studies are reported in Hinze's book.¹¹ Of particular note are the measurements by Klebanoff of the turbulence intensity close to the wall¹² (i.e., $z/\delta \leq .02$). Measurements on a smooth wall of both mean velocity and the longitudinal component of turbulence intensity for zero, adverse and favorable pressure gradients are reported by Schloemer.¹³ Data for a flow with zero pressure gradient on smooth and rough walls are reported by Blake¹⁰ and by Burton.¹⁴ Finally, measurements on both smooth and rough walls in a range of pressure gradients is given by Burton.¹⁵ This latter reference is particularly useful in that the profiles of turbulence intensity in several directions are given for these boundary layers.

Specific parameters of the boundary layer flows selected for this study are given in Table I. The corresponding turbulence intensity and mean velocity data are discussed in subsequent sections.

2. Data Curve Fit

a. Turbulence Intensity

The analytical model which involves a numerical integration across the boundary layer requires the profile of turbulence intensity. This profile is defined by the experimental measurements at a relatively small number of distances from the boundary. Furthermore in those data sets that include more than one component of the turbulence intensity, the measurement locations can differ for each component. When more than one turbulence velocity component is reported, we use the following definition for the turbulence intensity:

$$u' = \left[\frac{\sum_{i=1}^N (u_i')^2}{N} \right]^{1/2} \quad (18)$$

where u_i' is the root-mean-square turbulence velocity in the i^{th} direction and N components are measured (i.e., $N = 1, 2, \text{ or } 3$).

In order to use the discrete measurements in the analytical model, we must fit a continuous curve through the data points. Once such a curve has been defined, the data can be interpolated at any location between measurement points. Spline interpolation is used for this purpose. A cubic spline is a third-order polynomial that fits through two data points. The set of splines selected to span the data is then constrained to result in a function having minimum curvature. This constraint results in adjacent polynomials being joined continuously with continuous first and second derivatives (see Ref. 16 for further discussion and FORTRAN program).

The generation of an interpolating function for the turbulence intensity data occurs in two steps. First separate spline fits are made to the data for each component of the turbulence intensity, this being necessary for those cases where the measurement locations differ for each component. The specific sets of data used are shown in Fig. 1. The number of data points for each component typically varies from 10 to 15, and the data range between $z/\delta \approx .05$ and $z/\delta \approx 1.0$. The second step is to use these functions to calculate the turbulence intensity according to Eq. 1. Except for the data of Ref. 12 (see Fig. 2) there are no measurements available to define the variation of intensity near the wall. It is therefore assumed that the behavior in all boundary layers

is similar to that of the zero pressure gradient flow along a smooth wall. Specifically it is assumed that for $z/\delta < 0.05$ the dependence on distance from the wall is as follows:

$$u' = u' \Big|_{\hat{z}=0.05} e^{-(\hat{z}/.05)^2} \quad (19)$$

where $\hat{z} = z/\delta$. The measured data away from the wall along with the above assumption near the wall are used to generate the turbulence intensity profile at approximately 20 points spanning the range of z/δ from 2×10^{-4} to 1.2.

b. Mean Velocity Shear

With the possible exception of the flow in an adverse pressure gradient the mean velocity profile near the wall is well represented by a universal logarithmic distribution of the form,¹⁷

$$\frac{U(z)}{u_*} = 2.5 \ln(z/k_s) + B \quad (20)$$

where k_s is the equivalent sand roughness and B is a parameter depending on the hydraulic roughness of the wall (see Fig. 3). When the wall is hydraulically smooth (i.e., roughness height less than the viscous sublayer thickness), B is given by

$$B = 2.5 \ln \left(\frac{u_* k_s}{\nu} \right) + C \quad (21)$$

where ν is the kinematic viscosity of the fluid, and C is given by various sources to be in the range of 4.5 - 5.5. Substituting of Eq. 21 into Eq. 20 results in the familiar form of the universal distribution for smooth walls, namely,

$$\frac{U(z)}{u_*} = 2.5 \ln \frac{u_* z}{\nu} + C \quad (22)$$

For completely rough walls B takes on a constant value of 8.5.

The mean velocity shear of all boundary layers having a velocity profile given by Eq. 20 is the same, namely,

$$\frac{dU}{dz} = 2.5 \frac{u_*}{z} \quad (23)$$

It is obvious that this relationship does not apply in the immediate proximity of the wall. In the case of a smooth wall, there is a constant stress layer where the mean shear can be related to the shear velocity and the fluid viscosity. Since the mean shear profile is multiplied in the analytical model by the profile of turbulence intensity which vanishes at the wall, a complete description of the mean shear is not required.

The universal velocity distribution in Eq. 20 does not extend to the outer reaches of the boundary layer. To account for the outer region, the expression in Eq. 20 can be made non-universal by adding the correction term provided by Cole's law of the wake. This term can be adjusted to match the deviations from the universal law that are encountered with rough walls and with non-zero pressure gradients. However, in the outer region of the boundary layer both the turbulence intensity and the mean shear (see Eq. 23) become small. Furthermore, since these two profiles are multiplied together in the calculation, it is not necessary to include the shear contribution from the law of the wake term.

Equation 23 has been used for the mean velocity shear for all the boundary layers in zero and favorable pressure gradients. The flow in the adverse pressure gradient reported in Ref. 15 however is not found to follow a universal logarithmic distribution. For this flow the velocity distribution is reasonably well described by a power law,

$$u/U_o = (z/\delta)^{1/n} \quad (24)$$

with $n \approx 1.50$ for the flow with a free stream velocity of $U_o = 100$ ft/s (see Fig. 4). Using this form for the velocity profile along with the definition of the displacement thickness, we find that

$$\delta_1/\delta = \frac{1}{n+1} \approx 0.4 \quad (25)$$

The mean velocity shear in this boundary layer is given by

$$\frac{dU}{dz} = .667 \frac{U_o}{\delta} \left(\frac{\delta}{z} \right)^{.333} \quad (26)$$

This shear has a weaker dependence on distance from the wall than that of Eq. 23.

3. Data Interface with Numerical Integration

The numerical calculation of the shear-turbulence contribution to the correlation function requires the product of turbulence intensity and mean velocity shear. For convenience this product is evaluated at approximately 20 points from $z/\delta = 2 \times 10^{-4}$ to $z/\delta = 1.2$ using the spline fit to the turbulence data discussed in Section B.2 and the analytical expression for the mean shear discussed in Section B.2. A cubic spline fit to the product is made which is then called by the numerical integration routine.

The results for the turbulence intensity, mean velocity shear, and the product for flow with zero pressure gradient along smooth walls (Fig. 5); zero pressure gradient along rough walls (Fig. 6); favorable pressure gradient along smooth walls (Fig. 7); and adverse pressure gradient along smooth walls (Fig. 8). The outer integral in Eqs. 16 and 17 is evaluated using Simpson's rule. The number of terms required for convergence of these integrals is found to depend on the spatial separation.

C. Wavenumber Spectrum

The wavenumber spectrum is given by the two-fold cosine transformation of the correlation function (see Eq. 11). These integrals are evaluated using Filon's integration formula.¹⁸ The shear noise contribution to the correlation differs from the purely turbulence contribution in that it depends on the direction of spatial separation (e.g., flow or transverse). Because of this, the two-fold transformation of the shear noise contribution becomes a product of the one-dimensional transforms in each direction, that is,

$$\Phi(k_1, k_2) = 4P(\omega) \int_0^{\infty} R(\xi) \cos k_1 \xi d\xi \int_0^{\infty} R(\eta) \cos k_2 \eta d\eta \quad (27)$$

The narrowband spectrum level in Eq. 11 is assumed to be given by the point pressure spectrum (see for example Ref. 19).

IV. RESULTS

In this section results are presented for the point pressure, the spatial correlation functions, and the low wavenumber level of the four flows discussed in Section III. These boundary layers (viz., zero pressure gradient on smooth and rough walls, and both favorable and adverse pressure gradient flows on smooth walls) are selected to be representative of the range of variation of mean and turbulence profiles encountered in practice. Because of its highly non-planar flow, the boundary layer in the adverse pressure gradient is inconsistent with the basic assumptions of the analysis. It is of interest however to see whether the calculated results bear any resemblance with experimentally determined characteristics.

The root-mean-square (RMS) pressure normalized to the dynamic head is given by

$$\bar{P}/q = [C_{pp}(0)]^{1/2} \quad (28)$$

where $q = \frac{1}{2} \rho U_o^2$, and the "bar" indicates RMS value. If we normalized the pressure to the wall shear stress then the following relationship is found:

$$\bar{P}/\tau_w = \frac{1}{2} \left(\frac{U_o}{u_*} \right)^2 [C_{pp}(0)]^{1/2} \quad (29)$$

Measurements of this quantity by a number of investigators in boundary layers with nominally zero pressure gradient are found to be in the range,²⁰

$$\bar{P}/\tau_w = 3 \pm 1 \quad (30)$$

Values of this ratio have been calculated for the four flows examined in this study. Both the shear and turbulence contributions to the point pressure have been calculated. A summary of these results is given in Table II where the total pressure and the shear contribution are compared with experimentally determined values. For all four boundary layers the turbulence term contributes at most 11 percent to the total RMS point pressure. This is consistent with the findings of Ref. 3. With the exception of the flow under the adverse pressure gradient, the calculated results are within the range given by Eq. 30 and are in reasonable agreement with the specific experimental determination.

The normalized spatial correlation function in both the flow and transverse directions is plotted in Figs. 9 thru 12 as a function of separation distance normalized to displacement thickness. Based on the results of the point pressure calculations, only the shear contribution to the correlation functions has been evaluated. The results for the flow over the smooth wall in zero pressure gradient shown in Fig. 9 indicate a positive correlation in the transverse direction for all separations and a correlation in the flow direction that changes sign at a normalized separation of approximately 3.5. In general the magnitude of the correlation in the transverse direction exceeds that in the flow direction, this being consistent with the broadband measurements of Ref. 9 and 21. The results for the correlation in the flow direction display a long region of negative correlation that slowly returns to zero at large separation. This result in general gives a somewhat negative average to the correlation (and by Parseval's theorem, to the level at zero wavenumber) in the flow direction. This result violates the Kraichman-Phillips theorem (i.e., Eq. 7). Since there is no experimental information available in the range of very low wavenumbers (i.e., in and somewhat above the acoustic range) and since the effects of this negative average are less important at somewhat higher wavenumbers, this aspect of the results is not thought to adversely effect the comparison among flows. The most likely reason for the long region of negative correlation is the error introduced by implementing the procedure to calculate the correlation function via the tabulated values given in Ref. 3. Specifically, the behavior of the correlation function at large separation depends on the values of several functions at large argument. Interpolation of these functions between the tabulated values is therefore a likely source of error.

In Fig. 10 the correlation functions are shown for the boundary layer flow in zero pressure gradient over a rough wall. These correlation functions are minimally different from those of the smooth wall flow shown on Fig. 9. The principle difference is found in a larger point pressure for the rough wall flow (see Table II). The normalized correlation functions shown in Fig. 11 for the flow over the smooth wall in the favorable pressure gradient are also similar to those obtained for the zero gradient flow.

Figure 12 shows the results for the correlation functions in the boundary layer on a smooth wall in an adverse pressure gradient. As discussed above calculations of this non-planar flow are not expected to agree well with measurements. The correlation in the flow direction has a deep region of negative correlation compared with the results obtained for the previous flows. Additionally, even the transverse correlation is somewhat negative at large separations.

Results for the low wavenumber-frequency spectrum are presented on Figs. 13 thru 16 for the four flows. These results are calculated via Eq. 27 at a Strouhal number ($S = \omega \delta_1 / U_0$) of unity. For each flow the normalized spectrum is plotted against dimensional wavenumber for a range of low wavenumbers that is above the acoustic wavenumber (ω / c_0) for frequencies below approximately 800 Hz. Also presented on these figures is the zero wavenumber level calculated for these flows using a modified Corcos spectrum. At a Strouhal number of unity for these flows this spectrum is essentially independent of wavenumber with the normalized level being given by

$$\frac{\phi(0,0,\omega)U_0}{q^2 \delta_1^3} = \frac{8}{\pi^2} \frac{C_1^3}{C_3} \left(\frac{U_c}{U_0} \right)^2 \left(\frac{u^*}{U_0} \right)^4 S^{-3} (1+C_1^2)^{-2} \quad (31)$$

where the ratio of convection to external velocity is taken to be 0.6 and the constants are $C_1 = .08$ and $C_3 = .55$.

On Fig. 13 the wavenumber spectrum is shown for the zero pressure gradient boundary layer on a smooth wall. The increasing slope at low wavenumbers is a result of the somewhat negative value at zero wavenumber. At the higher wavenumber range the level is approximately 12 dB above that of the modified Corcos level. The level for the zero pressure gradient flow over the rough wall shown on Fig. 14 is found to be approximately 16 dB above the smooth wall result and approximately 20 dB higher than the Corcos spectrum. The level of the spectrum calculated for the favorable pressure gradient flow shown on Fig. 15 is approximately 27 dB higher than that of the zero pressure gradient flow along the smooth boundary, and it is substantially higher than that derived from the modified Corcos spectrum. It should be noted that the latter spectrum has been defined by adjusting the Corcos spectrum to agree at low wavenumber with available measurements, these resulting from flows in nominally zero

pressure gradient on smooth walls. It is therefore not unreasonable to expect a poor comparison with the modified Corcos spectrum for the flows with non-zero pressure gradient. Figure 16 shows the results for the flow in an adverse pressure gradient.

V. CONCLUSIONS

The objective of this study has been to explore the utility of an approximate procedure for evaluating the effects of flow non-ideality on the narrowband characteristics of the wall pressure field, specifically on the wavenumber-frequency spectrum at low wavenumbers. The procedure which is "exact" for broadband results but approximate for narrowband spectra has been implemented using partial results available in tabular form in Ref. 3. Conclusions drawn from this study are the following:

1. The RMS point pressure normalized to the wall shear stress that is obtained for three of the flows is in reasonable agreement with the experimentally determined value. The value obtained for the flow in a substantially adverse pressure gradient is considerably larger than that measured.
2. The levels of the low wavenumber spectra are somewhat higher than the levels obtained from the modified Corcos spectrum for the two zero pressure flows. Substantial differences are obtained between these two spectra for the flows in non-zero pressure gradients.
3. The calculated spectra at very low wavenumbers are contaminated by errors introduced by the use and interpolation of the tabulated functions. This finding is detrimental to a more general usage of the method.

TABLE I
BOUNDARY LAYER PARAMETERS

Flow	U_o (ft/s)	δ (ft)	δ_1 (ft)	u^*/U_o	$\bar{k}_g^{(a)}$ (ft)	$\frac{\delta_1}{q} \frac{dp}{dx}$
Smooth Wall/ Zero Pressure Gradient ¹⁴	164	.142	2.3×10^{-2}	.034	0	0
Rough Wall/ Zero Pressure Gradient ¹⁴	164	.200	4.6×10^{-2}	.055	7.7×10^{-3}	0
Smooth Wall/ Favorable Pressure Gradient ¹⁵	164	.039 ^(b)	4.9×10^{-3}	.049	0	-9.2×10^{-4}
Smooth Wall/ Adverse Pressure Gradient ¹⁵	100	.180 ^(c)	7.2×10^{-2}	.022	0	19

(a) Arithmetic mean roughness height

(b) Assumed to be $8 \delta_1$

(c) See Eq. 25

TABLE II
CALCULATED RATIO OF RMS SURFACE PRESSURE TO WALL SHEAR STRESS

Flow	u^*/U_o	$C_{pp}(0)$	\bar{P}/τ_w		
			Calculated		Measured
			Total	$C_{pp}^{(1)}$	
Smooth Wall $\nabla P = 0$	0.034	7.2×10^{-5}	4.1	3.7	3.6
Rough Wall $\nabla P = 0$	0.055	4.7×10^{-4}	3.8	3.6	2.9
Smooth Wall Favorable ∇P	0.049	1.5×10^{-4}	2.7	2.5	2.1
Smooth Wall Adverse ∇P	0.022	4.5×10^{-5}	68	67	8

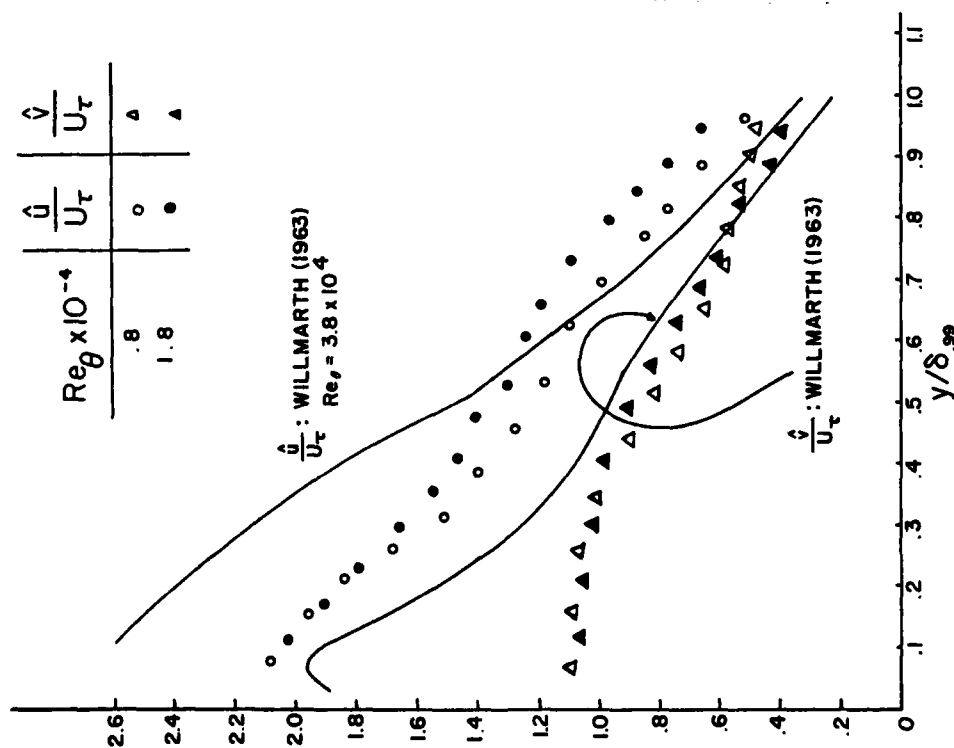


Fig. 1a - Relative turbulent intensities --
smooth wall.

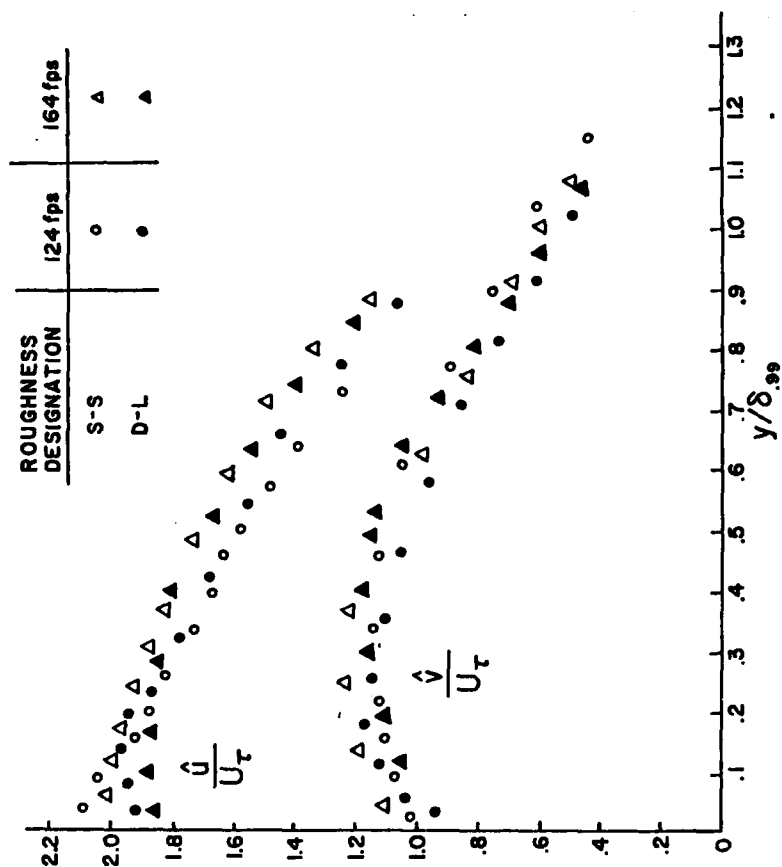


Fig. 1b - Relative turbulent intensities --
rough walls.

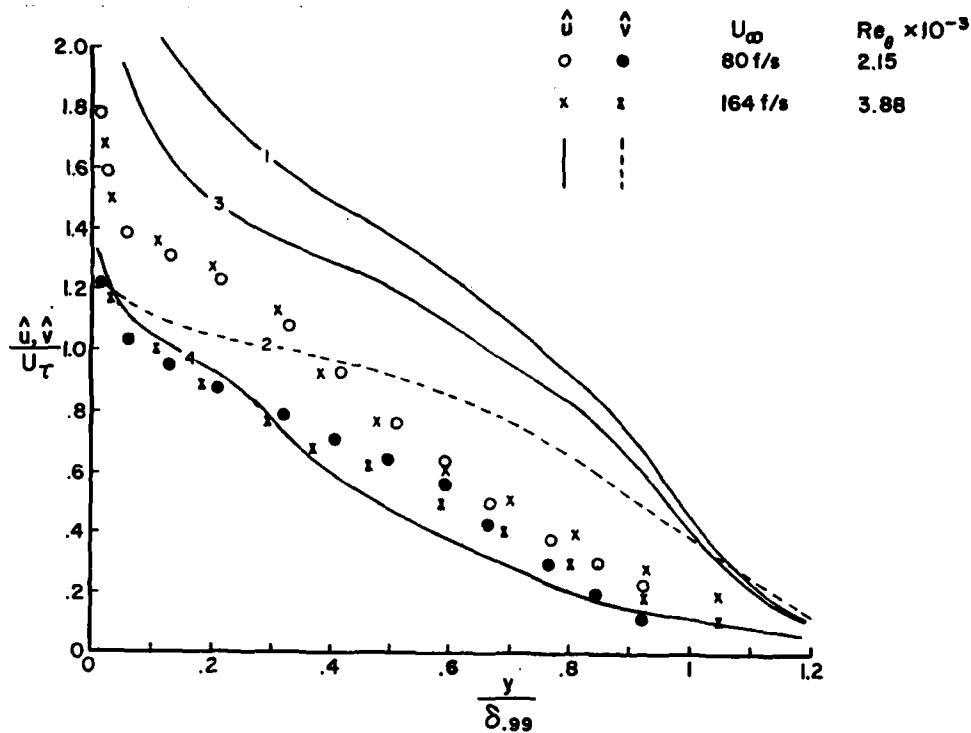


Fig. 1c - Turbulent Velocity Intensities over Smooth Walls. Symbols: Favorable Gradient:

- (1) \hat{u} no gradient, Blake (1970) (3) \hat{u} no gradient, Schloemer (1966)
 (2) \hat{v} no gradient, Blake (1970) (4) \hat{u} favorable, Schloemer (1966)

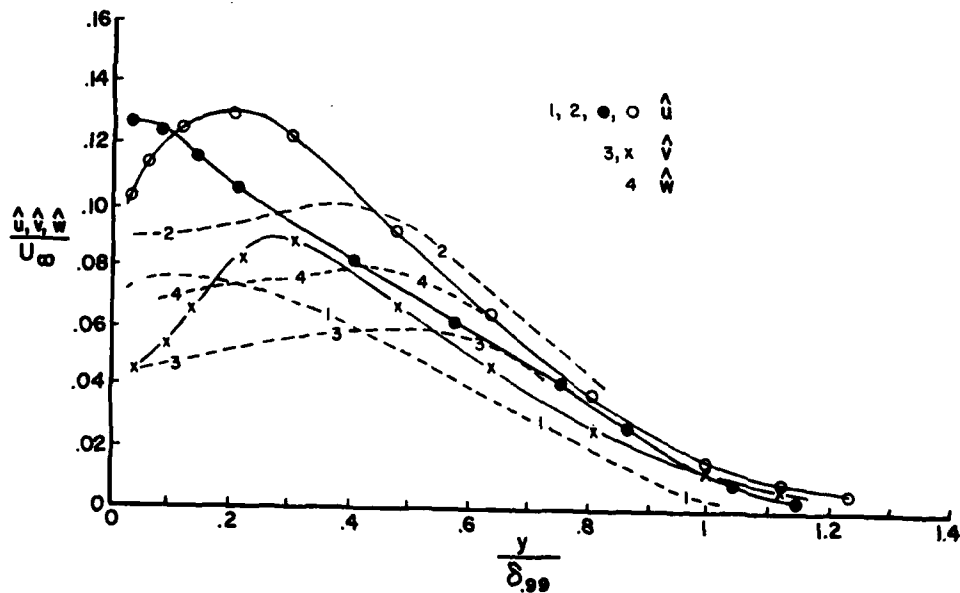


Fig. 1d - Turbulent Velocity Intensities over Smooth Walls with Adverse Gradients.

- (1) \hat{u} , Schloemer (1966) (3) \hat{v} , Bradshaw (1966)
 (2) \hat{u} , Bradshaw (1966) (4) \hat{w} , Bradshaw (1966)

Filled circles: $\xi = 0$. Other points: $\xi = 24.3$

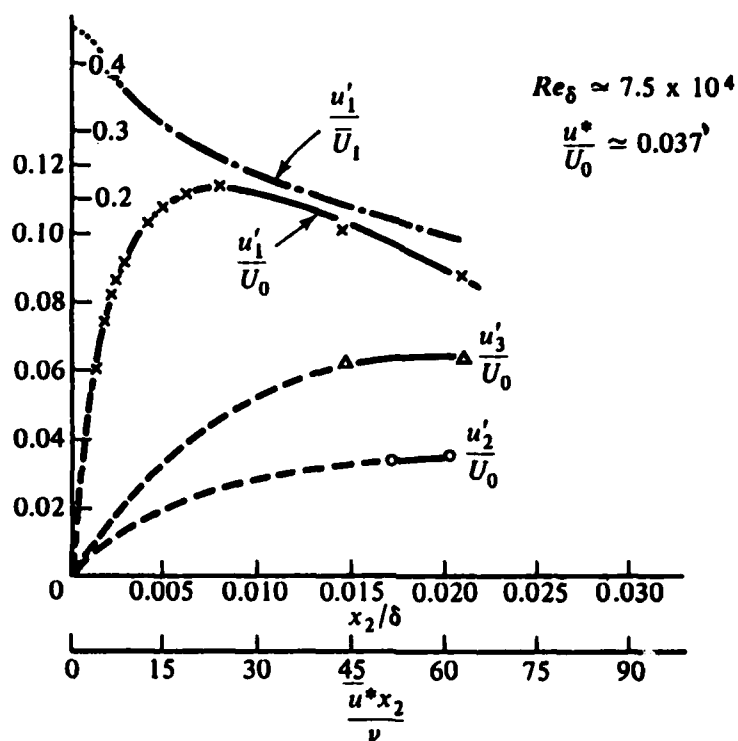


Fig. 2 - (a) Variation of turbulence kinetic energy across the boundary layer.
 (b) Variation of turbulence intensity near the wall.¹⁴

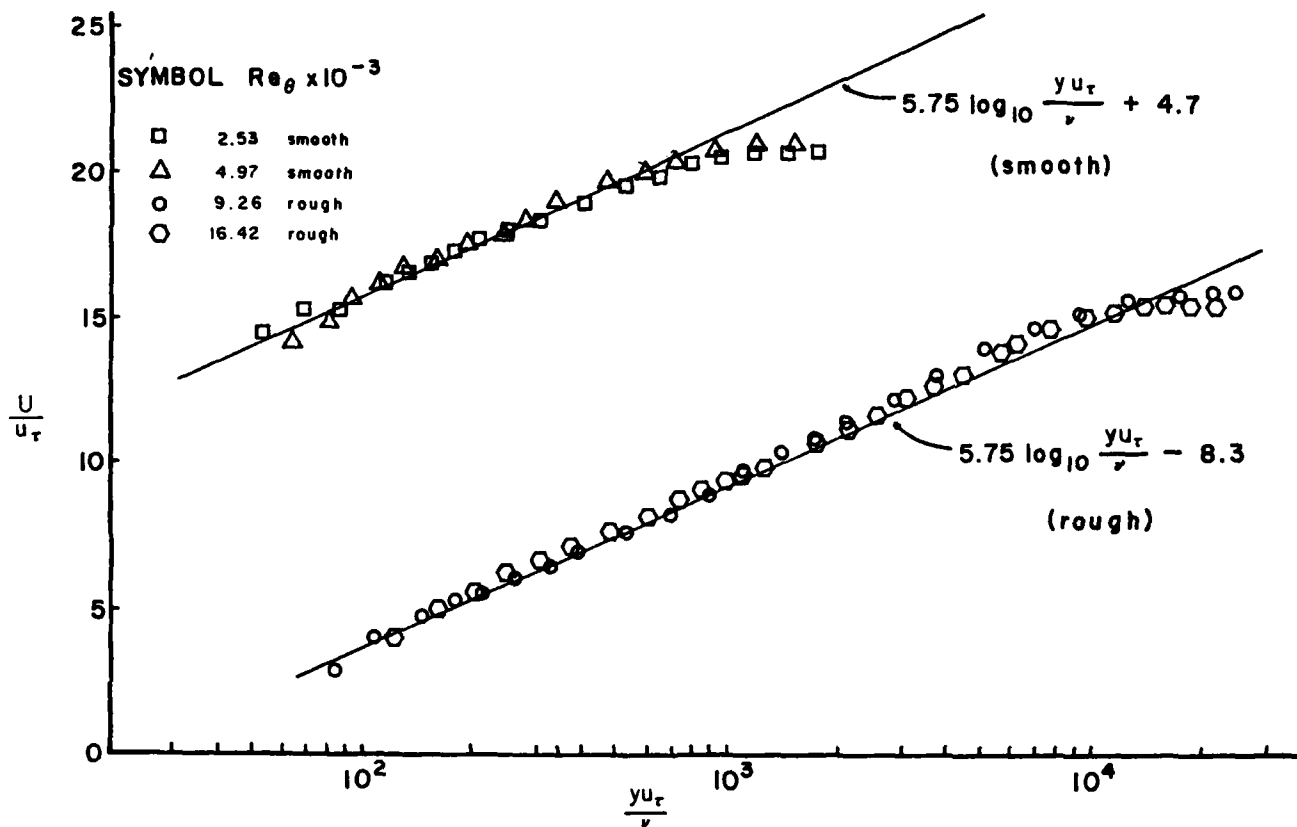


Fig. 3 - Mean velocity profiles with inner parameter scaling. Favorable gradients.¹³

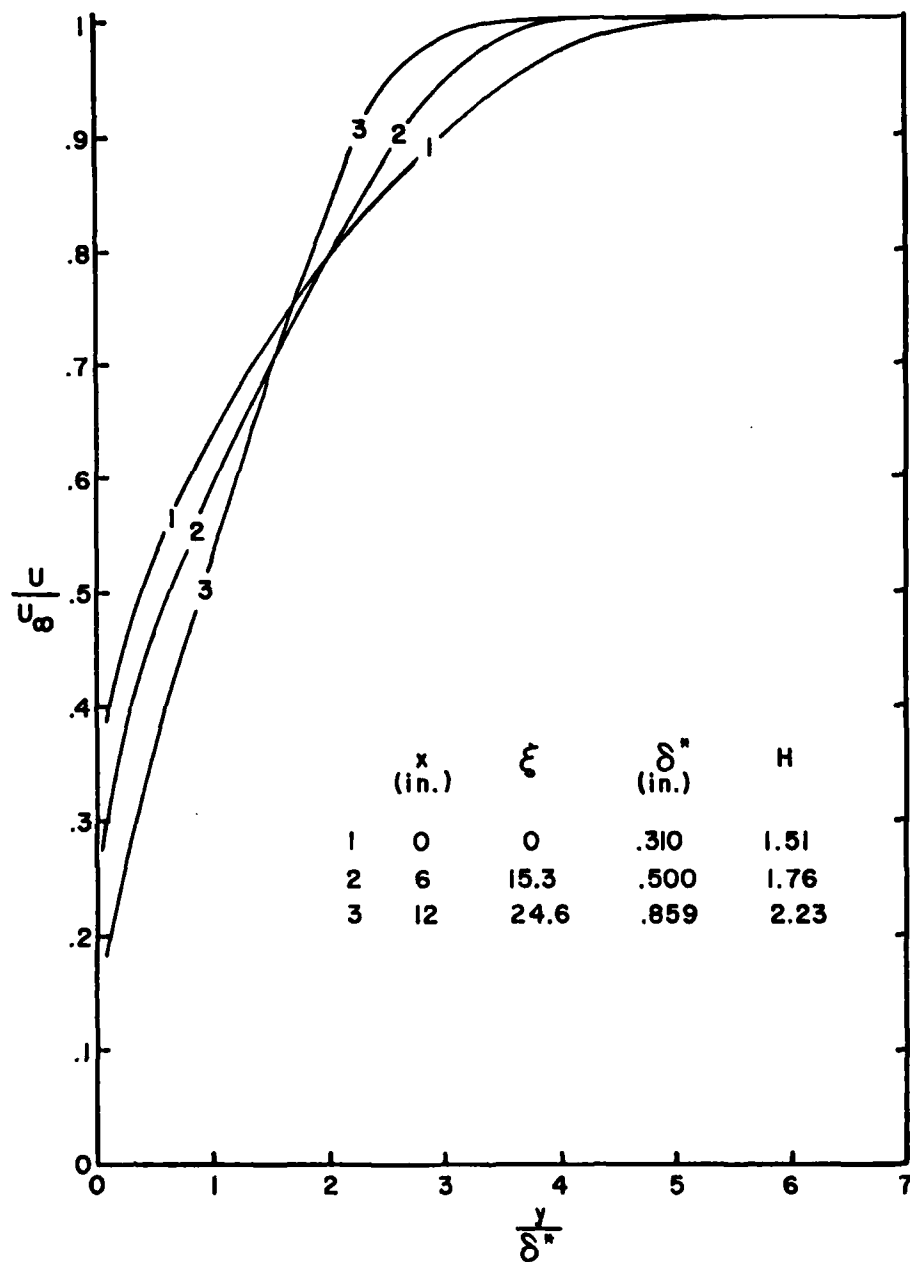


Fig. 4 - Mean velocity profiles with outer parameter scaling. Adverse gradient and smooth wall.¹⁵

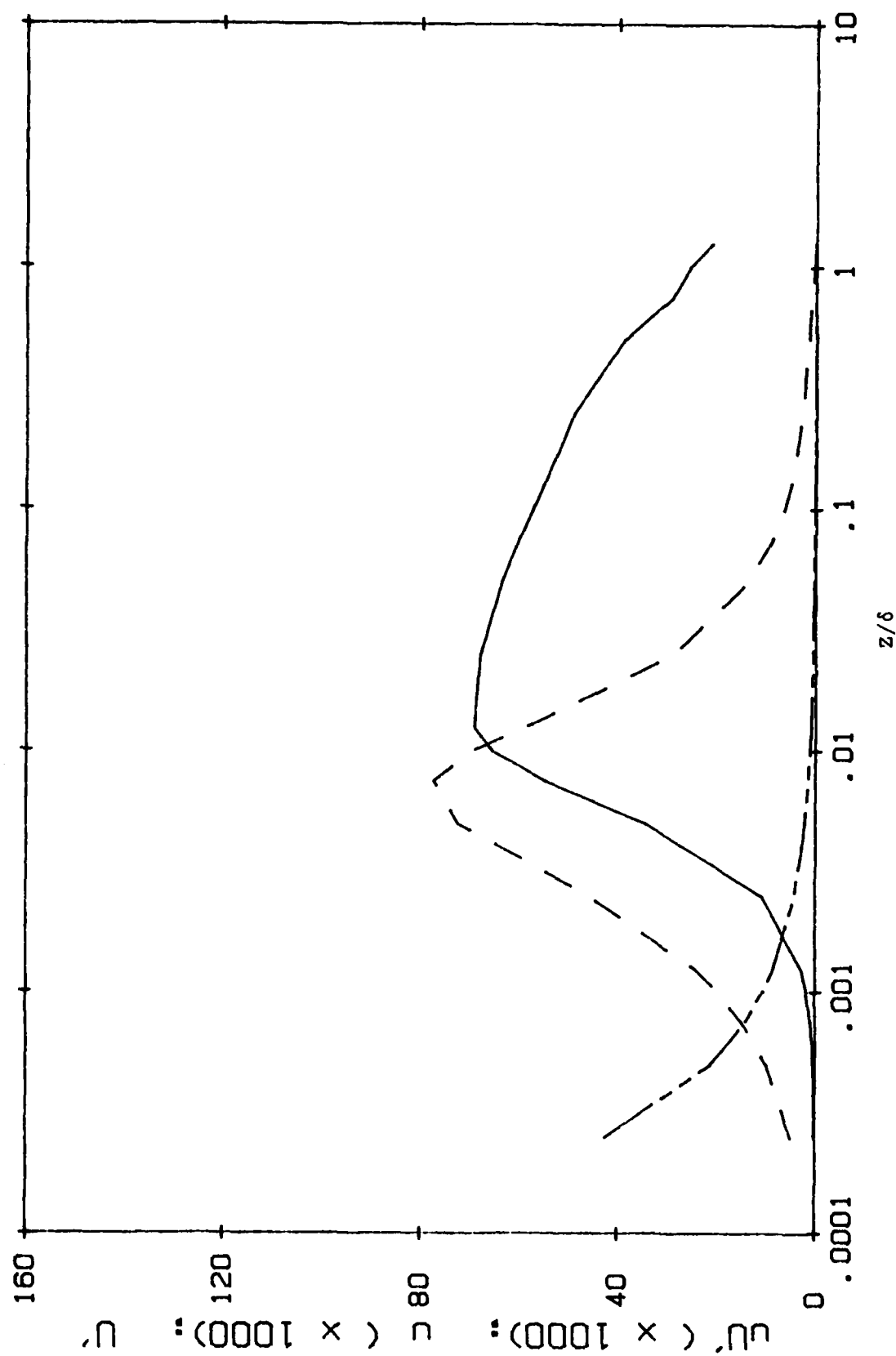


Fig. 5 - Profiles of normalized mean velocity shear (— — —), turbulence intensity (— — —), and their product (— · —) across the boundary layer. (Smooth wall; zero pressure gradient.)

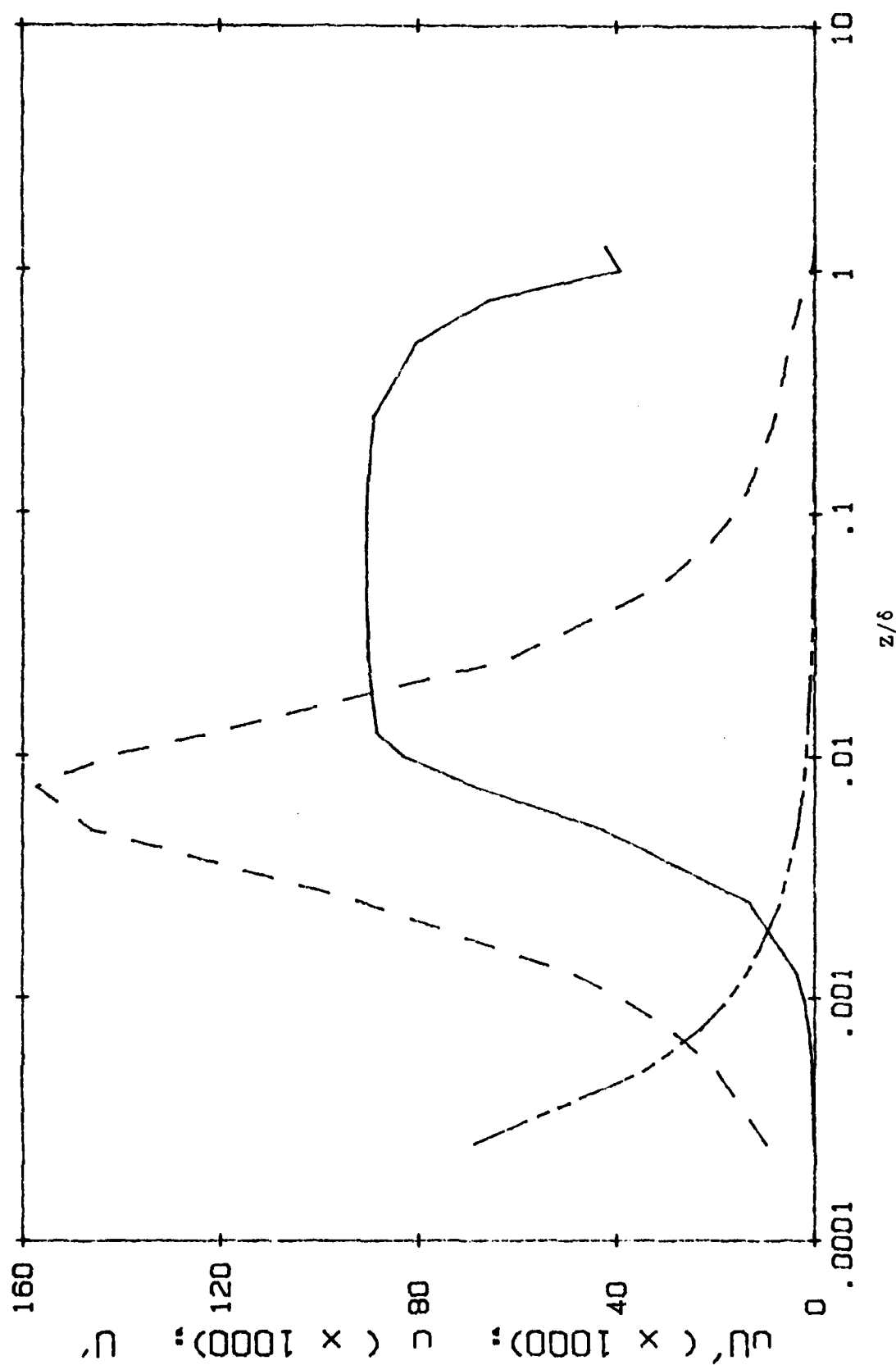


Fig. 6 - Profiles of normalized mean velocity shear (—), turbulence intensity (---), and their product (-·-·-) across the boundary layer. (Rough wall; zero pressure gradient.)

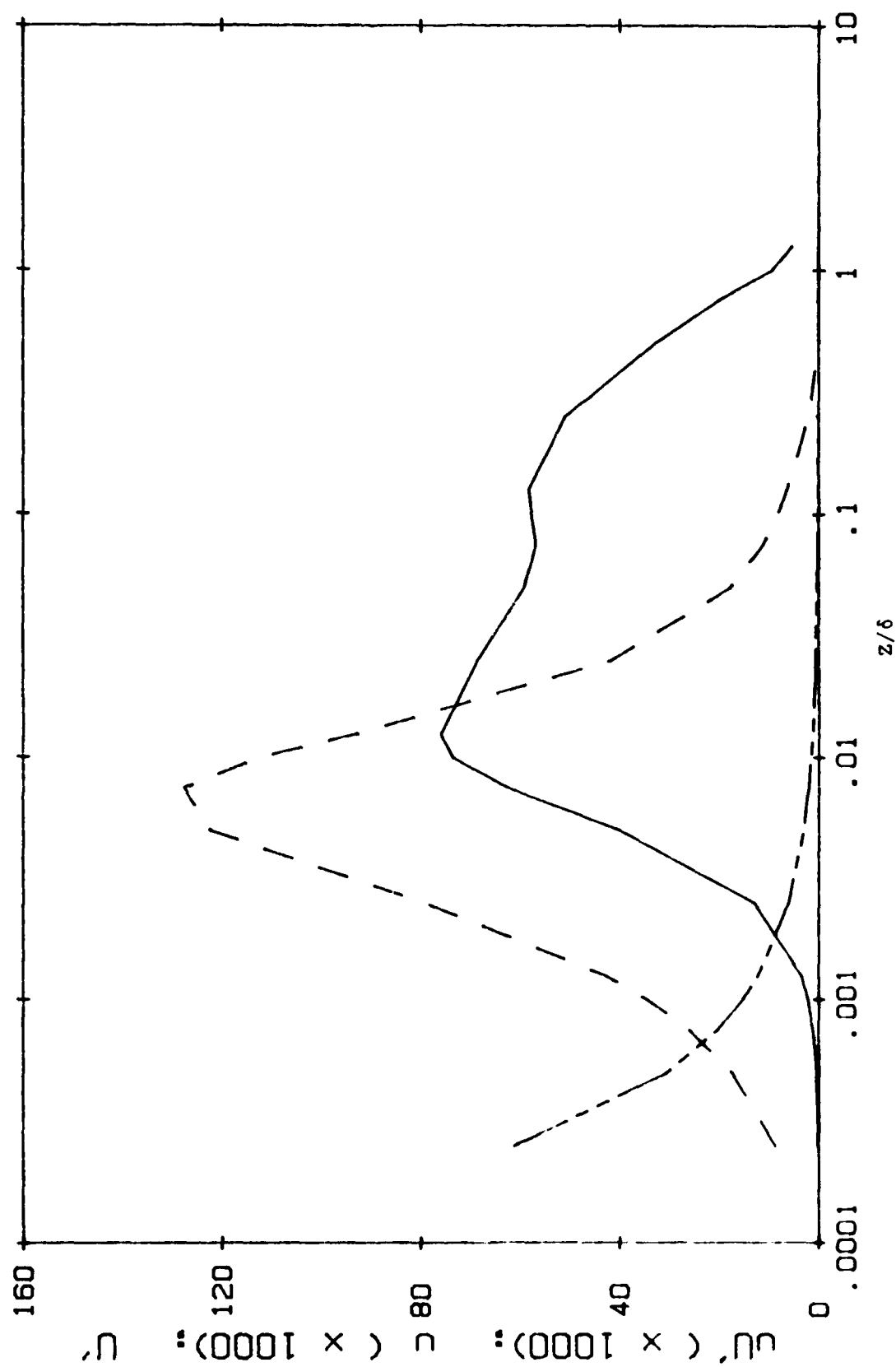


Fig. 7 - Profiles of normalized mean velocity shear (—), turbulence intensity (---), and their product (-·-·-) across the boundary layer. (Smooth wall; favorable pressure gradient.)

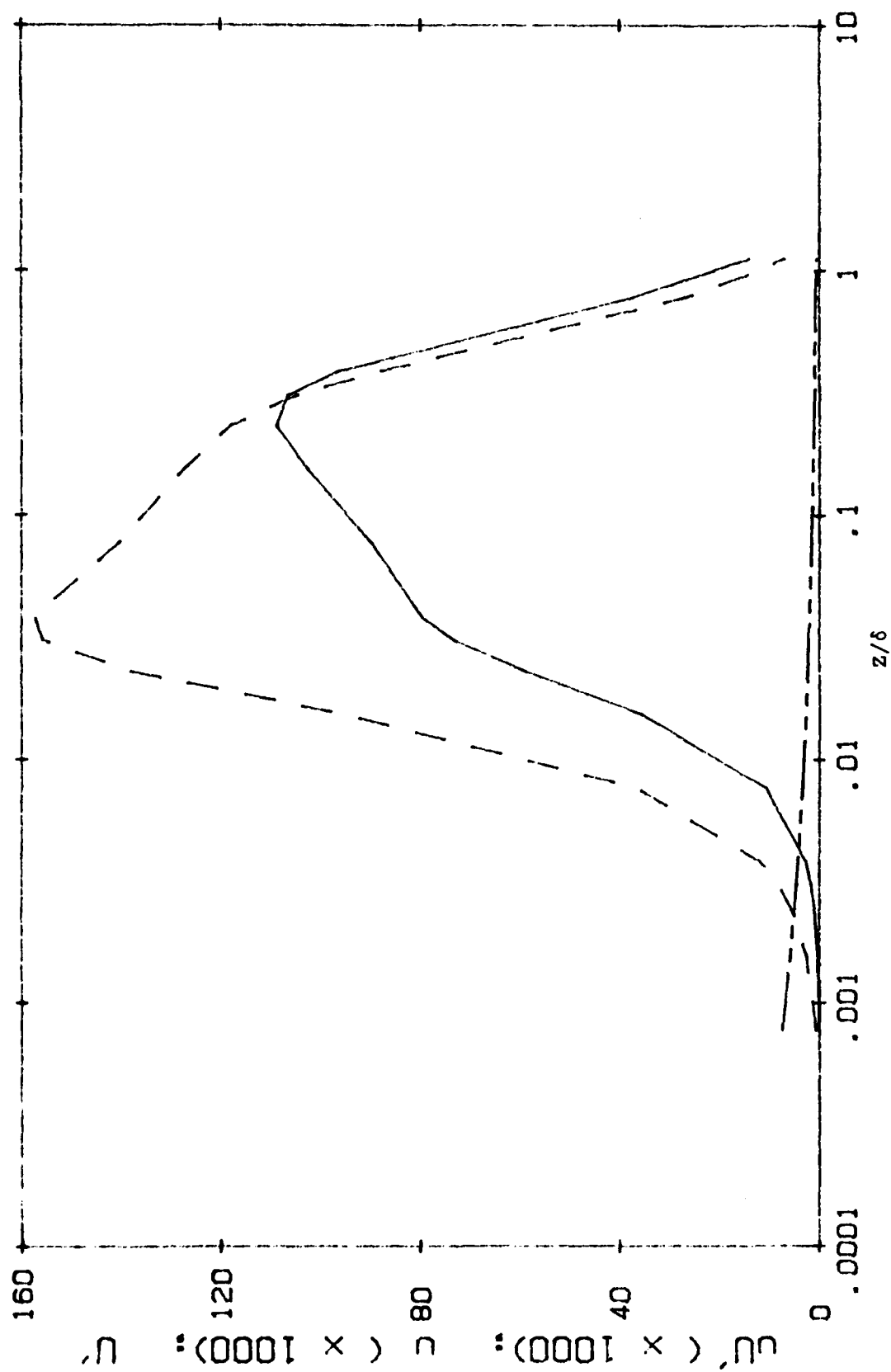


Fig. 8 - Profiles of normalized mean velocity shear (—), turbulence intensity (---), and their product (-----) across the boundary layer. (Smooth wall; adverse pressure gradient.)

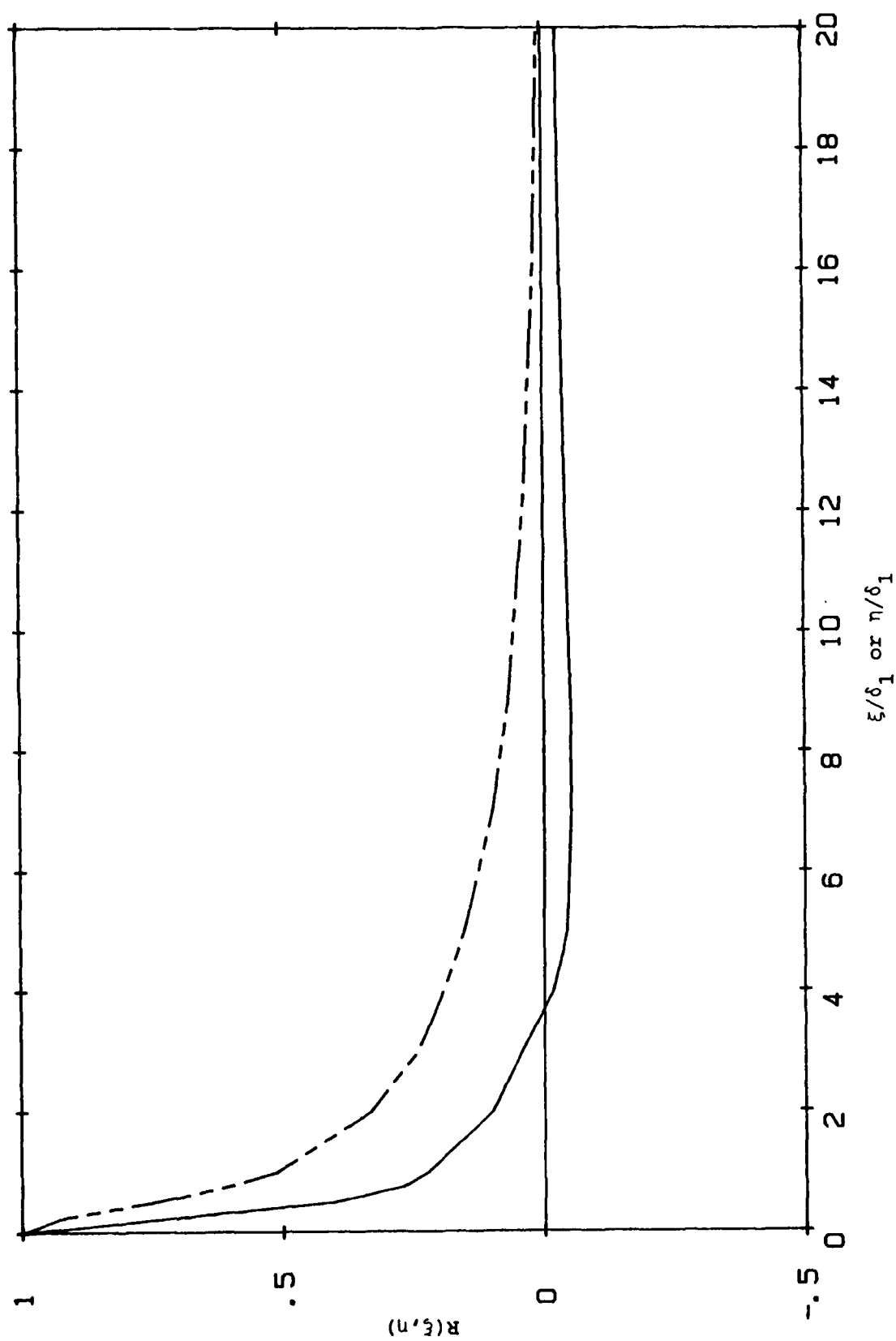


Fig. 9 - Normalized spatial correlation function in the flow (—) and transverse (---) directions. (Smooth wall; zero pressure gradient.)

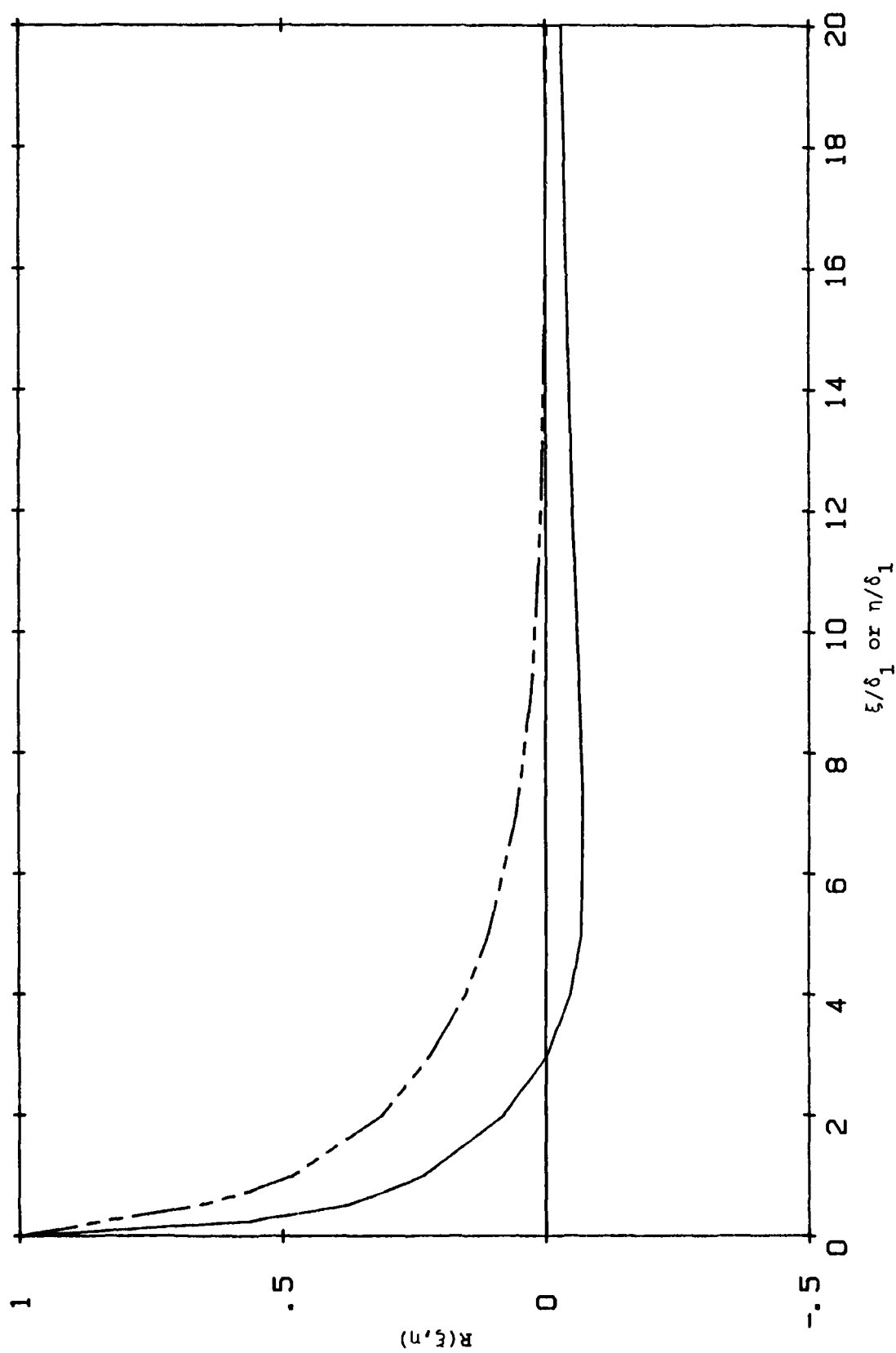


Fig. 10 - Normalized spatial correlation function in the flow (—) and transverse (---) directions. (Rough wall; zero pressure gradient.)

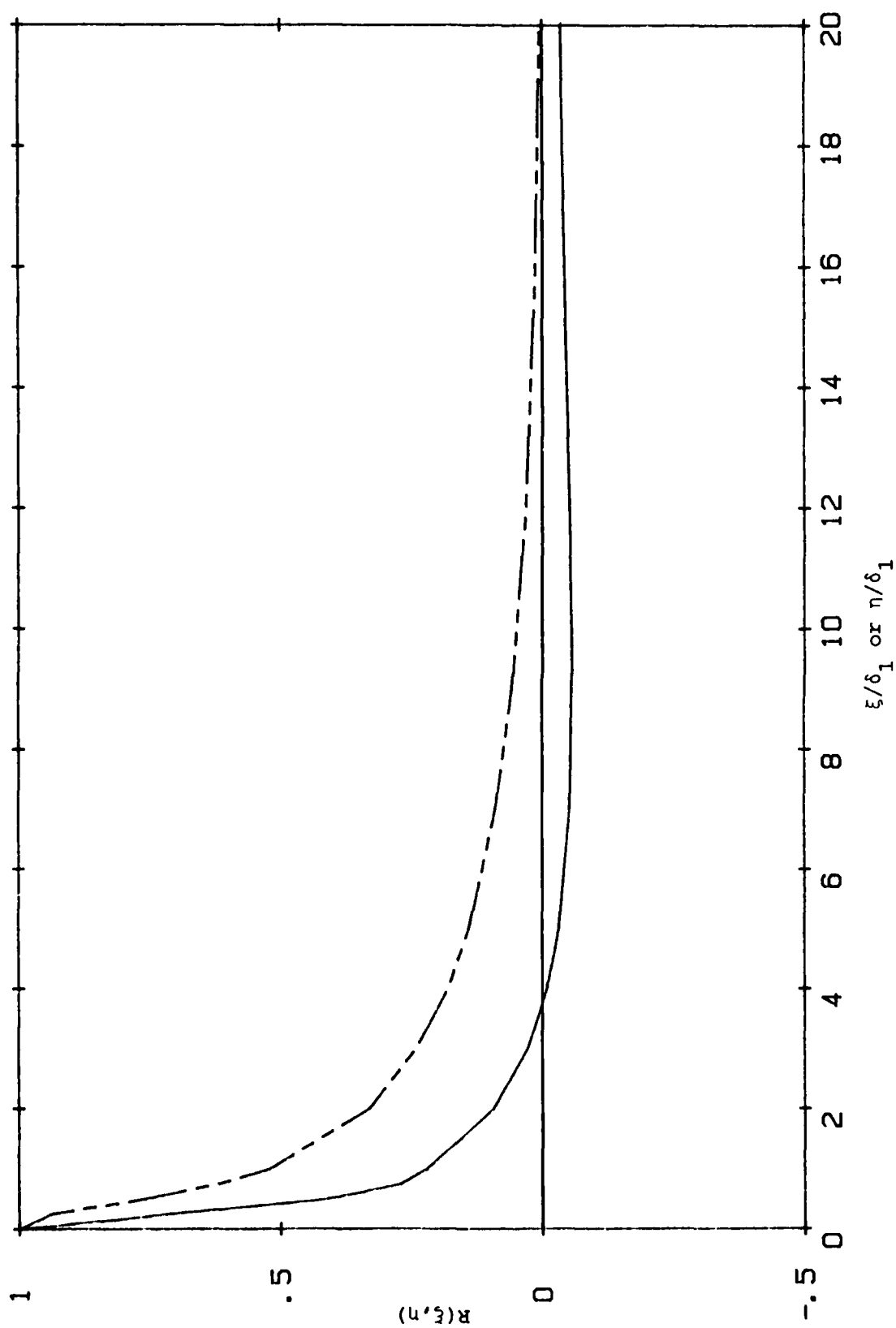


Fig. 11 - Normalized spatial correlation function in the flow (—) and transverse (---) directions. (Smooth wall; favorable pressure gradient.)

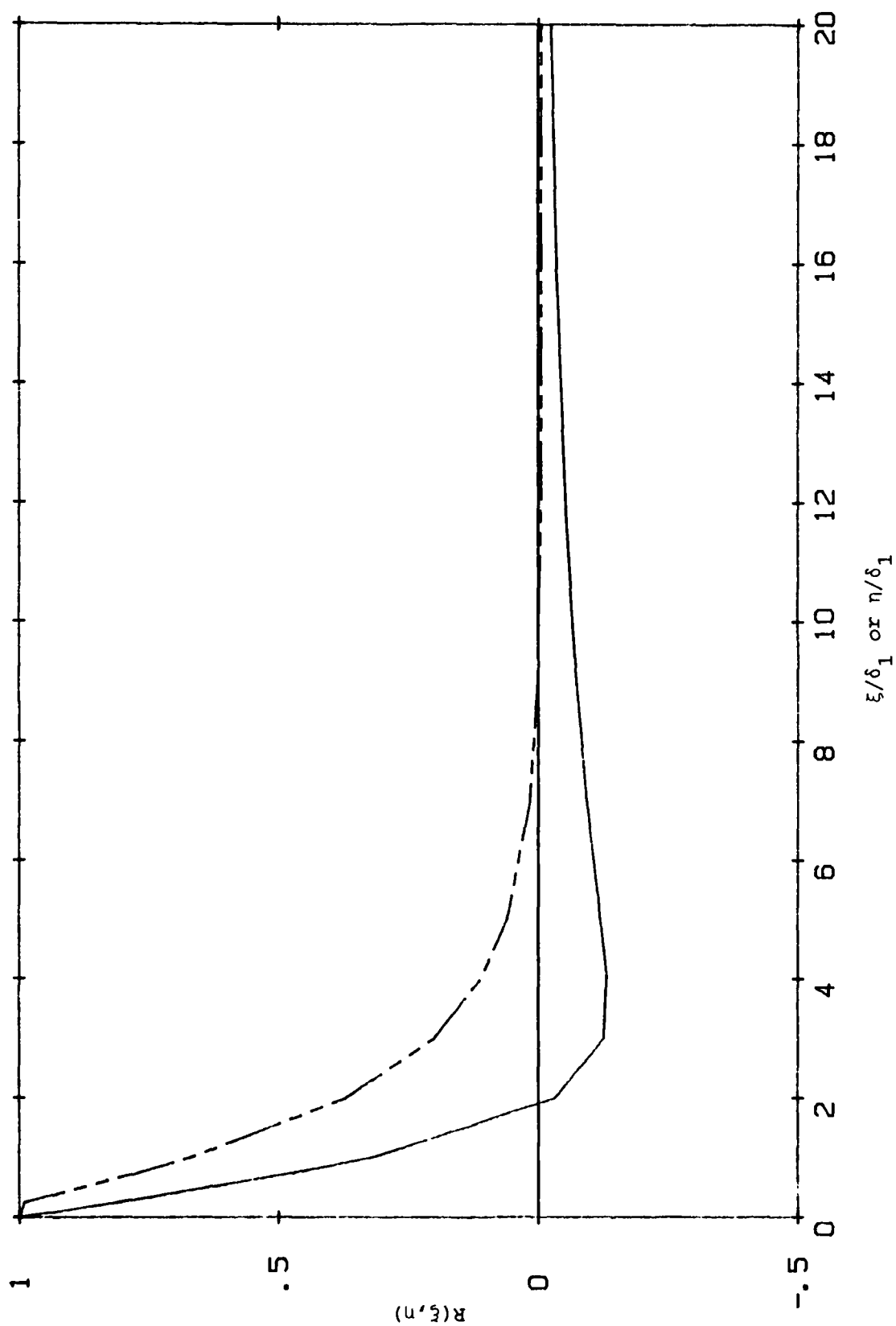


Fig. 12 - Normalized spatial correlation function in the flow (—) and transverse (---) directions. (Smooth wall; adverse pressure gradient.)

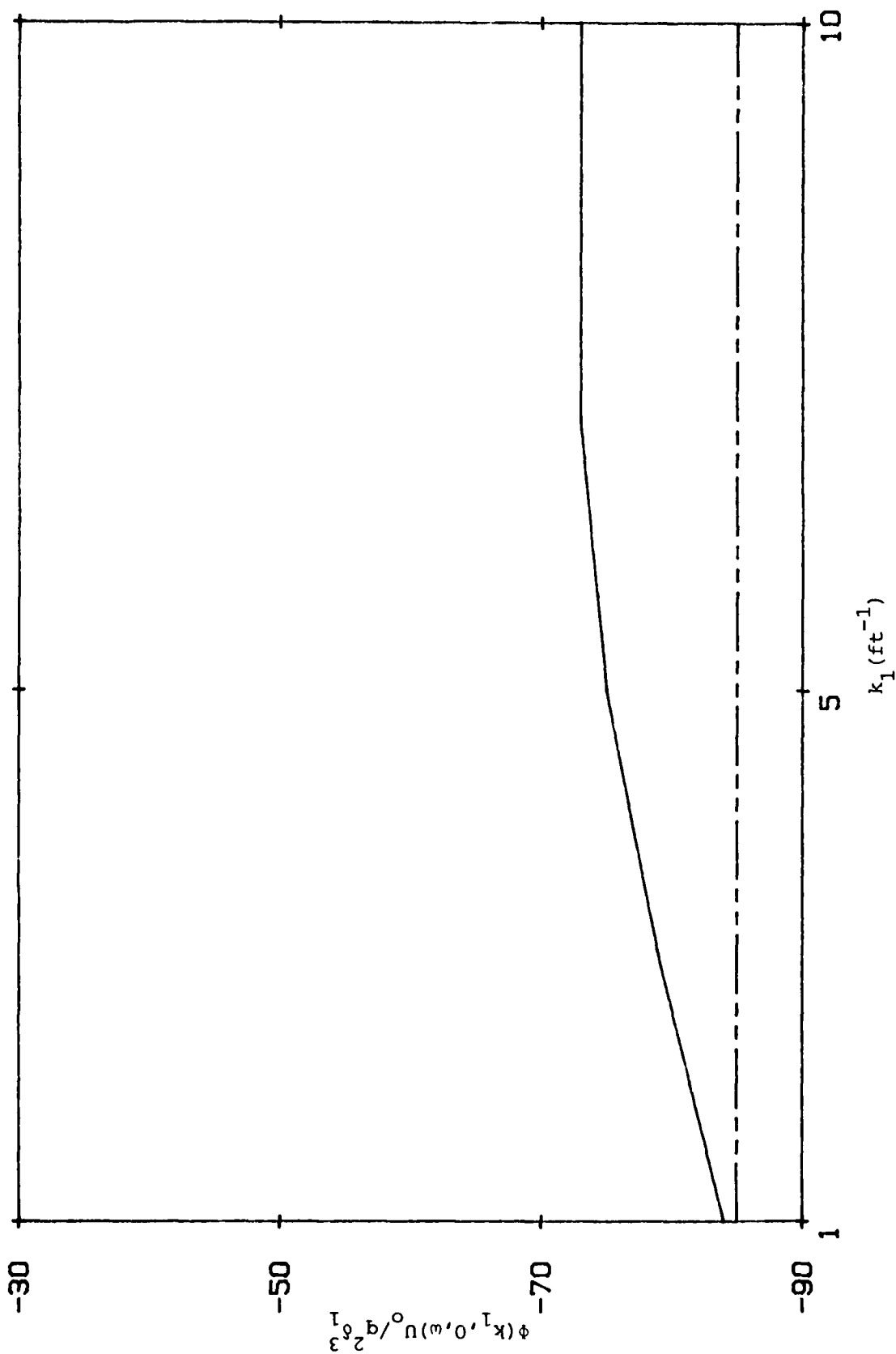


Fig. 13 - Normalized wavenumber spectrum at a Strouhal number of unity calculated using the present procedure (—) and the modified Corcos model (---). (Smooth wall; zero pressure gradient.)

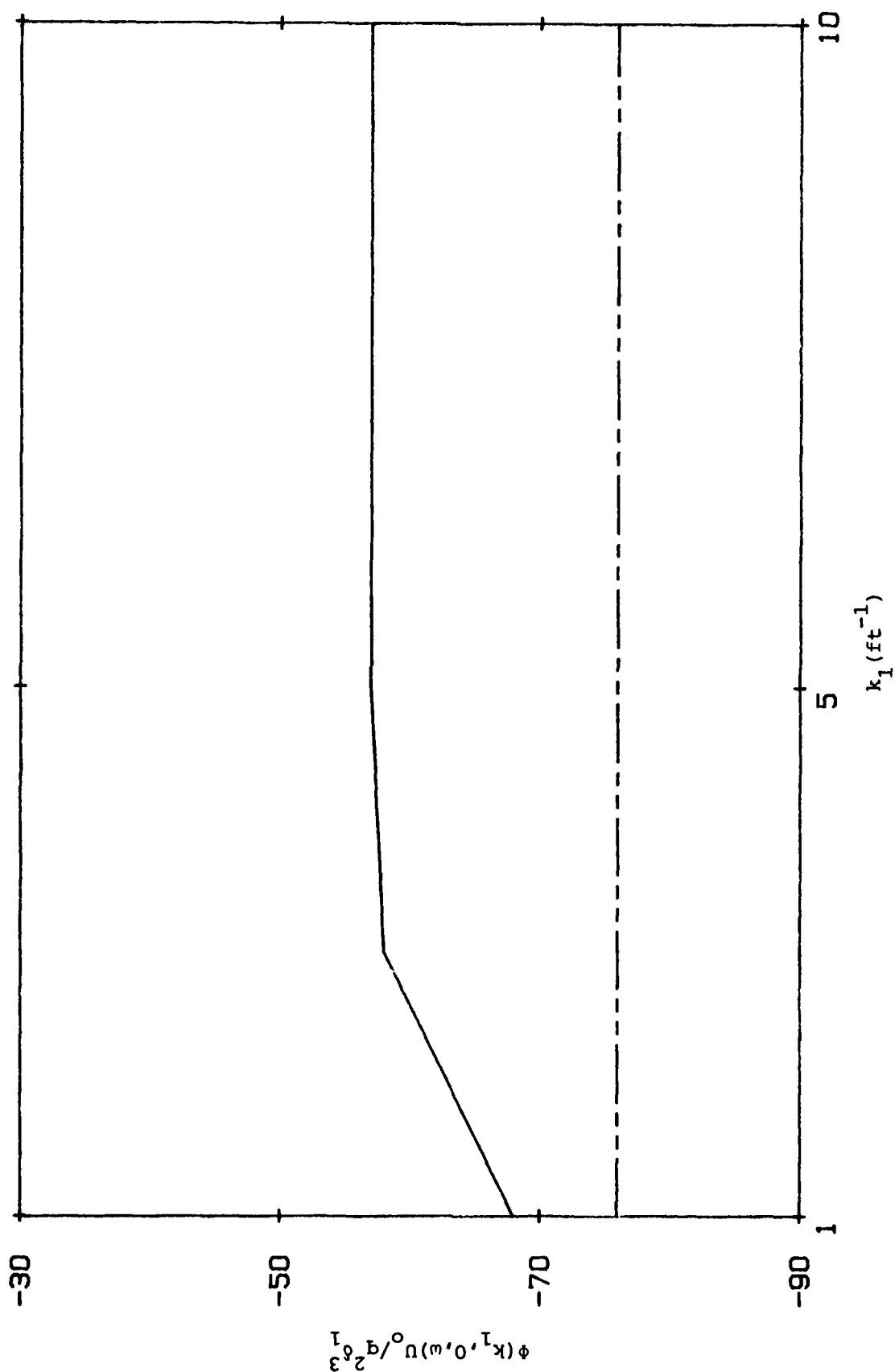


Fig. 14 - Normalized wavenumber spectrum at a Strouhal number of unity calculated using the present procedure (—) and the modified Corcos model (---). (Rough wall; zero pressure gradient.)

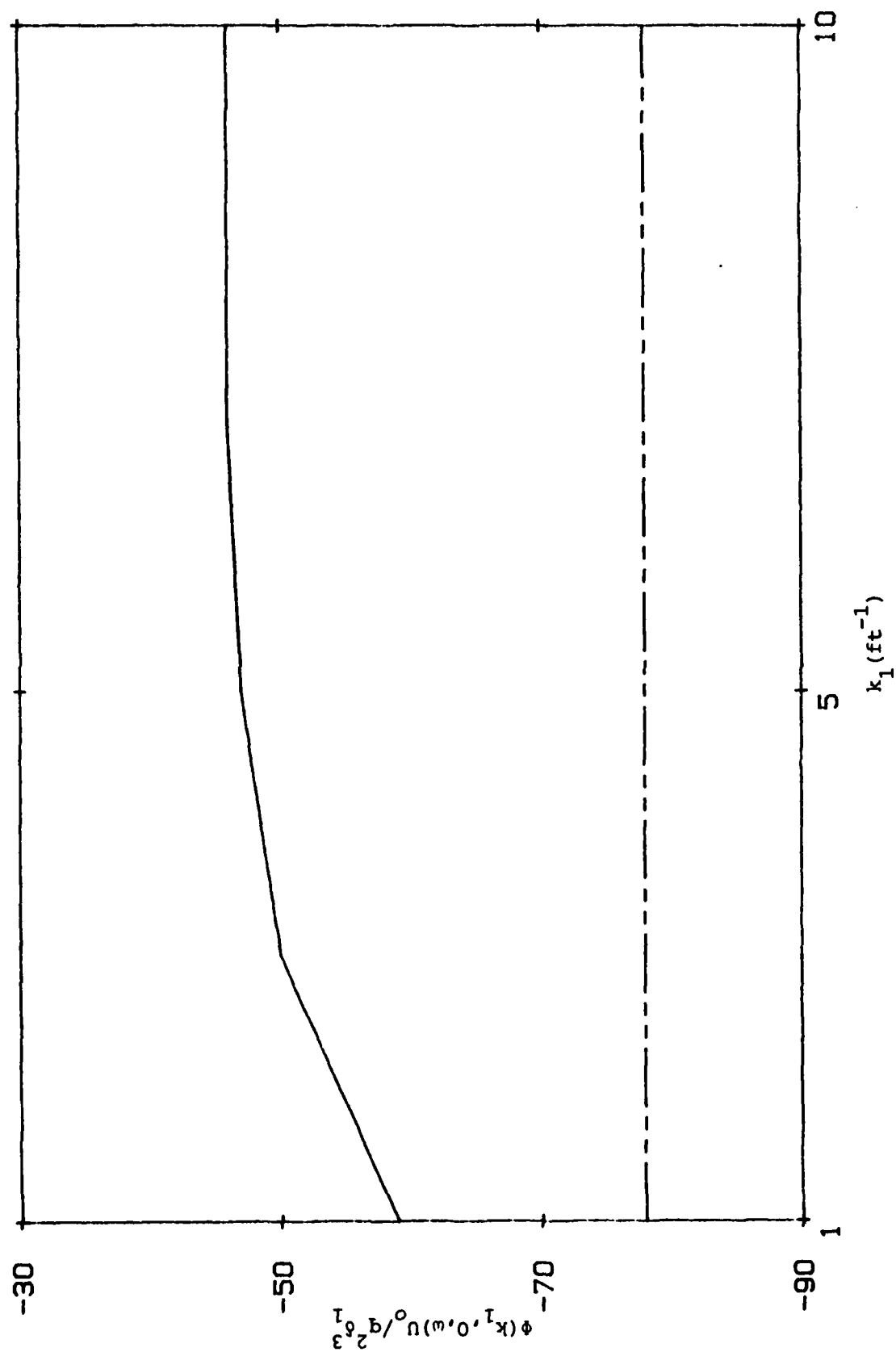


Fig. 15 - Normalized wavenumber spectrum at a Strouhal number of unity calculated using the present procedure (—) and the modified Corcos model (---). (Smooth wall; favorable pressure gradient.)

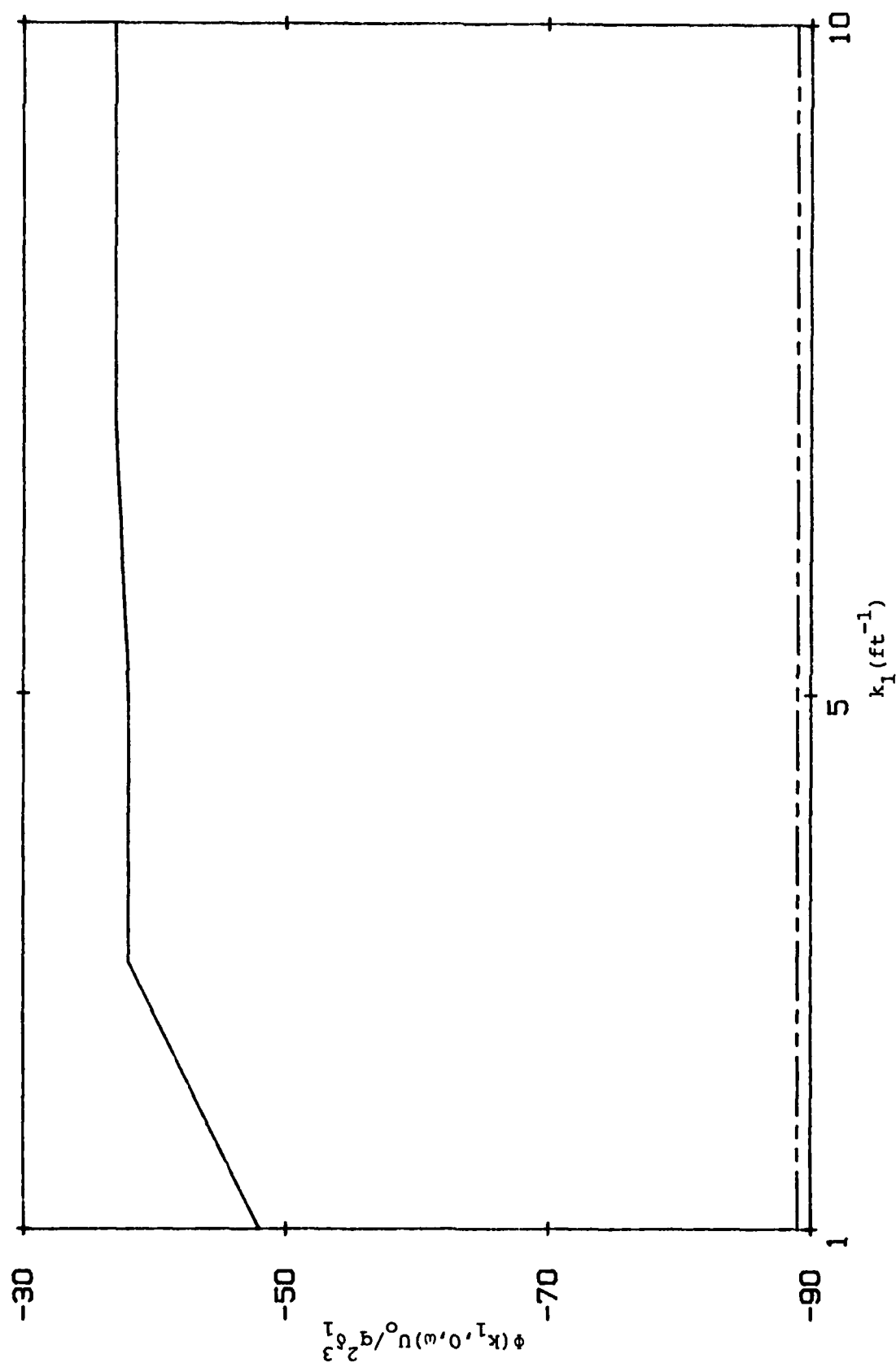


Fig. 16 - Normalized wavenumber spectrum at a Strouhal number of unity calculated using the present procedure (—) and the modified Corcos model (---). (Smooth wall; adverse pressure gradient.)

REFERENCES

- 1 T. M. Farabee and F. E. Geib, Jr., Measurement of Boundary Layer Pressure Fields with an Array of Pressure Transducers in a Subsonic Flow, David Taylor Naval Ship R&D Center Rept. 76-0031 (March 1976).
- 2 D. M. Chase, "Modeling the Wave Vector-frequency Spectrum of Turbulent Boundary Layer Wall Pressure", J. Sound Vib. 70 (1980) 29-67.
- 3 W. C. Meecham and M. T. Tavis, Theoretical Pressure Correlation Functions in Turbulent Boundary Layers, Rept. SAMSO-TR-78-42 prepared for Air Force Weapons Laboratory (June 1984). Also, Phys. Fluids 23 (1980) 1119-1131.
- 4 J. E. Cole, III, Spectrum of the Turbulent Boundary Layer Wall Pressure Fluctuations at low Wavenumber, CAA Rept. U-861-320.1 prepared for Office of Naval Research (October 1982).
- 5 R. H. Kraichnan, "Pressure Fluctuations in Turbulent Flow Over a Flat Plate", J. Acoust. Soc. Am. 28 (1956) 378-390. Also, see discussion in Ref. 2.
- 6 M. J. Fisher and P. O. A. L. Davies, "Correlation Measurements in a Non-frozen Pattern of Turbulence", J. Fluid Mech. 18 (1964) 97.
- 7 M. K. Bull, "Wall-pressure Fluctuations Associated with Subsonic Turbulent Boundary Layer Flow", J. Fluid Mech. 28 (1967) 719-754.
- 8 J. M. Clinch, "Measurements of the Wall Pressure Field at the Surface of a Smooth-walled Pipe Containing Turbulent Water Flow", J. Sound Vib. 9 (1969) 398-419.
- 9 W. W. Willmarth and C. E. Wooldridge, "Measurements of the Fluctuating Pressure at the Wall Beneath a Thick Turbulent Boundary Layer", J. Fluid Mech 14 (1962) 187.
- 10 W. K. Blake, Turbulent Boundary Layer Wall Pressure Fluctuations on Smooth and Rough Walls, MIT Acoustics and Vibrations Laboratory Rept. 70208-1 (January 1969).

- 11 J. O. Hinze, Turbulence, 2nd ed., (McGraw-Hill Book Co., New York, 1975), 626-642.
- 12 P. S. Klebanoff, National Advisory Committee on Aeronautics Tech Note No. 3178 (1954).
- 13 H. H. Schloemer, "Effects of Pressure Gradients on Turbulent-Boundary Layer Wall-Pressure Fluctuations", J. Acoust. Soc. Am. 42 (1967) 93-113.
- 14 T. E. Burton, On the Generation of Wall Pressure Fluctuations for Turbulent Boundary Layers Over Rough Walls, MIT Acoustics and Vibration Laboratory Rept. 70208-4 (March 1971).
- 15 T. E. Burton, Wall Pressure Fluctuations at Smooth and Rough Surfaces Under Turbulent Boundary Layers with Favorable and Adverse Pressure Gradients, MIT Acoustics and Vibration Laboratory Rept. 70208-9 (June 1973).
- 16 G. E. Forsythe, et al., Computer Methods for Mathematical Computations, (Prentice-Hall, Inc., Englewood Cliffs, NJ, 1975) 71-79.
- 17 H. Schlichting, Boundary Layer Theory, 6th ed., (McGraw-Hill Book Co., New York, 1968) 580-583.
- 18 M. Abramowitz and I. A. Stegun, Handbook of Mathematical Formulas, (NBS Applied Math. Series 55, 1964) 890.
- 19 J. O. Hinze, op cit., p. 674.
- 20 W. K. Blake, Aero-hydroacoustics for Ships, David Taylor Naval Ship R&D Center Rept. DTNSRDC-84/010 (June 1984) 733.
- 21 M. K. Bull, Properties of the Fluctuating Wall-pressure Field of a Turbulent Boundary Layer, AASE Rept. 234 (March 1963).

END

FILMED

10-85

DTIC